Applied Geochemistry 89 (2018) 59–74

Contents lists available at ScienceDirect

Applied Geochemistry

journal homepage: www.elsevier.com/locate/apgeochem

# Thermodynamics of the solid solution - Aqueous solution system (Ba,Sr,Ra)$SO_4$ + $H_2O$: I. The effect of strontium content on radium uptake by barite

V.L. Vinograd[a,*], D.A. Kulik[b], F. Brandt[a], M. Klinkenberg[a], J. Weber[c], B. Winkler[d], D. Bosbach[a]

[a] Institute of Energy and Climate Research (IEK-6) – Nuclear Waste Management and Reactor Safety, Research Centre Jülich GmbH, 52425 Jülich, Germany
[b] Paul Scherrer Institut, Laboratory for Waste Management, 5232 Villigen PSI, Switzerland
[c] Chemical Science Division, Oak Ridge National Laboratory, TN 37830, USA
[d] Goethe University, Frankfurt, Germany

ARTICLE INFO

Editorial handling by Prof. M. Kersten

*Keywords:*
Celestite
Barite
Radium sulphate
Solid solution
Regular mixing

ABSTRACT

Thermodynamic properties of mixing in the ternary (Ba,Sr,Ra)$SO_4$ solid solution are determined using first principles based total energy calculations and Monte Carlo simulations. Two levels of theory, which correspond to the regular mixing and the generalized Ising model, are considered. The results show that the regular mixing parameters increase along the row of Ba-Ra, Ba-Sr and Sr-Ra binary systems proportionally to the squared difference of molar volumes of the end-members. The magnitudes of pairwise interactions similarly increase along the same row, manifesting a tendency to short-range ordering (SRO). In the (Ba,Sr)$SO_4$ system the SRO effect is approximately equivalent to a 40% decrease in the value of the regular mixing parameter. The ternary solid solution is well described as a regular mixture with the binary parameters $W_{BaRa}$ = 2.47 ± 0.22, $W_{BaSr}$ = 4.95 ± 0.75 and $W_{SrRa}$ = 17.50 ± 1.40 kJ/mol. These values imply that admixing $RaSO_4$ to the (Ba,Sr)$SO_4$ solid solution stabilizes Ba-rich and destabilizes Sr-rich compositions. Consequently, an addition of a small amount of $RaSO_4$ to a Sr-rich solid solution leads to a nucleation of a Ba- and Ra rich phase. This phenomenon, predicted in our thermodynamic modelling study, is directly confirmed by our experiments on re-crystallizing a powder of celestite with traces of Ba in the presence of an aqueous Ra-bearing solution. At a measurably high content of Ra in the system Ra-uptake by celestite occurs via a formation of a Ra-rich phase. The aqueous concentration of Ra in such systems would be governed mainly by the common anion effect caused by the relatively high solubility of Sr-rich sulphates. At lower Ra contents the retention of Ra would be enhanced both by the common anion and the dilution effects. Our simulations with the GEM-Selektor code predict that the optimum condition for Ra uptake is achieved when the barite solid solution contains 10 ± 5 mol % of $SrSO_4$.

## 1. Introduction

The accumulation of $^{226}Ra$ in spent nuclear fuel is an important matter of concern in safety assessments of long-term disposal of nuclear wastes in deep geological formations (e.g. Grandia et al., 2008; SKB, 2011; Nagra, 2014). $^{226}Ra$ ($T_{1/2}$ = 1622 years) is expected to gradually build up in the waste as the decay product of $^{238}U$. The secular equilibrium with $^{238}U$ (the activity of a freshly mined U ore) would be reached in about $10^6$ years. However, an additional source of $^{226}Ra$ accumulation would be due to the decay of $^{238}Pu$ via $^{234}U$ and $^{230}Th$. Due to the relatively long half-life of $^{230}Th$ (75380 years) the activity of $^{226}Ra$ in the spent fuel would pass through a maximum after about $10^5$ years, and, in the time interval of $10^4$–$10^5$ years Ra would dominate the dose of the waste (SKB, 2011). As the containers are thought to maintain integrity for ~$10^4$–$10^5$ years (SKB, 2011; NAGRA, 1984), an event of a container failure may involve a release of a significant amount of Ra, which could potentially provide risks of ground water contamination. Recent thermodynamic modelling studies suggested, however, that these risks are significantly reduced if barium sulphate, $BaSO_4$, is present in the near field of the container or if it forms upon an interaction of the released substances with ground waters. Under such conditions, only a small fraction of Ra will migrate away from a repository, as the aqueous concentration of Ra will be controlled by a poorly soluble Ba-rich (Ba,Ra)$SO_4$ solid solution (Kulik et al., 2004; Bruno et al., 2007; Grandia et al., 2008; Vinograd et al., 2013). Direct experiments on barite re-crystallization in Ra-bearing aqueous solutions at 25 °C (Bosbach et al., 2010; Curti et al., 2010; Klinkenberg et al., 2014; Brandt et al., 2015) have shown that the newly-formed dilute (Ba,Ra)$SO_4$ solid solution retains most of radium. Detailed microscopic evidence of the Ra uptake is given in the study of Weber et al. (2017).

* Corresponding author.
*E-mail address:* v.vinograd@fz-juelich.de (V.L. Vinograd).

https://doi.org/10.1016/j.apgeochem.2017.11.009
Received 10 August 2017; Received in revised form 27 October 2017; Accepted 23 November 2017
Available online 24 November 2017
0883-2927/ 

The importance of solid solution formation for Ra-uptake reveals itself mostly via the dilution effect (Kulik et al., 2004; Bruno et al., 2007; Prieto et al., 2016). The aqueous solubility product $K_S$ of $RaSO_4$ for the reaction $RaSO_4 = Ra^{2+} + SO_4^{2-}$ is given by

$$K_S = a(Ra^{2+})a(SO_4^{2+})/a(RaSO_4) = a(Ra^{2+})a(SO_4^{2+})/(x\gamma), \quad (1)$$

where $x$ and $\gamma$ are the mole fraction and the activity coefficient of $RaSO_4$, respectively. Consequently,

$$a(Ra^{2+}) = K_S x\gamma/a(SO_4^{2+}). \quad (2)$$

Here we mention that throughout the text $RaSO_4$ should be understood as ether a component of a solid solution or as a pure solid $RaSO_4$ phase. The latter distinction is always made clear from the context. Therefore, the index $s$, e.g. in $RaSO_4$,s, is avoided for brevity. Eqn. (2) shows that the formation of a dilute ideal ($\gamma = 1$) solid solution with $x = 0.001$ would decrease the aqueous activity of Ra by three orders of magnitude. For this reason, the dilution in a solid solution with barite can efficiently retard aqueous migration of radium. Hence, the demonstration of thermodynamic stability of barite minerals within engineered and geological barriers becomes an important item for safety assessments. It is often assumed that even if primary barite is absent in the host rock, a certain amount of secondary barite could be formed at the contamination front due to the release of Ba that is contained within the nuclear waste (Grandia et al., 2008) and the sulphate contained in the ground water. It is likely that the formation of this secondary barite will precede a significant release of Ra. Indeed, the $^{226}Ra$ escape will be controlled by isotope equilibria with actinides, and thus will persist over a long time interval, while the escape of Ba, which is presumably contained in the spent fuel as oxide precipitates (Bruno and Ewing, 2006), will probably occur soon after the container failure.

Although a large portion of the released Ra could be taken up by secondary barite, its sorption capacity would likely be small compared to the capacity of Sr-containing sulphates present in a host rock. As natural alkali-earth sulfates typically form $(Ba,Sr)SO_4$ solid solutions (Hanor, 2000), a theoretical demonstration of the efficiency of Ra retention by natural sulfates requires a thermodynamic description of the ternary $(Ba,Sr,Ra)SO_4$ system. In prospective host rocks, such as the Opalinus clay formation (Switzerland) several generations of barite-type minerals has been described (Lerouge et al., 2014). The earlier generations, formed presumably during the burial stage of sedimentation, are represented by barite-rich solid solutions of a wide range of compositions, which typically occur among other diagenetic minerals filling out pores in bioclasts. The latest generation, formed predominantly along fault zones, is represented by celestite-rich varieties. In the Callovo-Oxfordian argillite at Bure (France), sulfates are mostly represented by celestites that contain from 7 to 16% of $BaSO_4$, (Lerouge et al., 2011). These and other observations show that pure $BaSO_4$ barite never occurs in natural clay rocks, thus the Ra sorption capacity should be assessed as a function of the celestite content.

Eqn. (2) shows that the effect of dilution is counterbalanced by the effect of non-ideal mixing, which is expressed by the value of $\gamma$. Our previous study (Vinograd et al., 2013) has allowed us to put constraints onto the value $\gamma$ in the binary $(Ba,Ra)SO_4$ system. Our atomistic simulations showed that the mixing in this system is characterized by a very small degree of non-ideality ($\gamma \approx 3$), and consequently, the Ra-uptake by a pure $BaSO_4$ barite is very efficient. On the other hand, qualitative arguments suggest that $\gamma$ would likely increase with the Sr/Ba ratio. It can be assumed that due to a large difference in the sizes of $Ra^{2+}$ and $Sr^{2+}$, the mixing within the $(Sr,Ra)SO_4$ binary system will be very limited. Consequently, a high Sr/Ba ratio in barite would have a negative effect on Ra retention. However, a higher solubility of celestite, and, conceivably, an increase in the sulphate ion concentration in the aqueous phase with an increase in the Sr/Ba ratio, would help to keep $Ra^{2+}$ in the solid phase. The relative significance of these effects can only be assessed via thermodynamic modelling, for which the knowledge of the thermodynamics of mixing in the ternary system is required.

Up to now, the thermodynamic mixing properties of the $(Ba,Sr,Ra)SO_4$ solid solution remain poorly constrained. Particularly little is known about the effects of mixing in the binaries containing $RaSO_4$. The experimental and theoretical effort has been mostly focused on the $(Ba,Sr)SO_4$ solid solution – aqueous solution (SSAS) system (see Hanor (2000) for a detailed review). From the synthesis of the whole range of $(Ba,Sr)SO_4$ compositions at ambient conditions, it was inferred that this solid solution is thermodynamically ideal (e.g. Brower and Renault, 1971). On the other hand, Galinier et al. (1989), based on dissolution experiments, argued for a moderate degree of non-ideality, which is equivalent to a positive regular model interaction parameter $W_{BaSr}$ of $4.0 \pm 0.3$ kJ/mol. Similar estimates of 4.5–6.2 kJ/mol were derived from energy-volume relationships by Malinin and Urusov (1983). More recently, Becker et al. (2000), using the force-field model of Allan et al. (1993), arrived at a significantly larger effective $W_{BaSr}$ value of ~8.3 kJ/mol. Zhu (2004), using an energy vs. volume correlation and available estimates of $W$ values from co-precipitation experiments for various host-trace barite-type pairs, arrived at a value of $W_{BaSr}$ of about 3.8 kJ/mol. The same study allowed the estimation of the mixing parameters in other binaries: $W$ values of ~1.2 and ~8.1 kJ/mol for $(Ba,Ra)SO_4$ and $(Sr,Ra)SO_4$, respectively, were obtained. Vinograd et al. (2013), based on ab initio calculated defect formation energies, arrived at $W$ values of ~2.5, ~8.4, and ~19.9 for $(Ba,Ra)SO_4$, $(Ba,Sr)SO_4$ and $(Sr,Ra)SO_4$, respectively.

The last set of parameters is further refined in the present study. Complementing the previous study, we make a consistent attempt to take into account effects of short-range and long-range ordering (SRO and LRO). Here we show that magnitudes of the pairwise interactions, which are responsible for the SRO and LRO, in the binary systems of $(Ba,Ra)SO_4$, $(Ba,Sr)SO_4$ and $(Sr,Ra)SO_4$ are proportional to the magnitudes of the $W$ parameters. Modelling of the effects of ordering is performed here within the frame of the generalized Ising model. We find that the mixing properties within the $(Ba,Sr)SO_4$ binary are especially sensitive to the effect of SRO. Including this effect into models helps to partially resolve the controversy regarding the values of $W_{BaSr}$ parameters reported in the literature.

The aim of this study is threefold. First, we evaluate a consistent set of the mixing parameters for $(Ba,Sr,Ra)SO_4$. Second, with the aid of the GEM-Selektor modelling package (http://gems.web.psi.ch), we apply this model to simulate certain scenarios relevant for the retention of Ra by rocks containing barite minerals with variable Sr/Ba ratios at ambient temperature. An extension to elevated temperatures is described in a companion paper (Vinograd et al., 2017). One of these scenarios predicts that an equilibration of a Sr-rich $(Ba,Sr)SO_4$ solid solution with an aqueous Ra-bearing solution may lead to a nucleation of a minor phase, which is simultaneously rich in Ba and Ra. Third, we use a direct experimental approach to test the model prediction. Specifically, we equilibrate a powder of celestite that contains traces of $BaSO_4$ with a Ra-bearing aqueous solution and search for the presence of newly-formed Ra-rich crystals.

## 2. Methods

### 2.1. Atomistic simulations

The regular mixing model requires a single (Margules) interaction parameter $W_{AB}$ for an (A,B)$L$ binary system, where $L$ is an arbitrary ligand. The application of this model makes sense when the exchangeable atoms (A and B) are thought to be essentially disordered, while the enthalpy of mixing is approximately symmetric with respect to the midpoint of the composition domain. When the enthalpy is asymmetric, two Margules parameters, $W_{AB/A}$ and $W_{AB/B}$, can be defined. These parameters can be determined experimentally, e.g. via a drop solution calorimetry, or computed with the aid of atomistic

models as explained below.

The regular (subregular) model provides a sufficiently accurate description of the thermodynamics of mixing of an (A,B)$L$ solid solution in cases when one of the components is present in a small amount (i.e. $x_A < 0.1$ or $x_B < 0.1$). Such solid solutions can be considered to be essentially disordered. At intermediate compositions various effects of short- or long-range order typically become important. An adequate description of these effects becomes possible with the generalized Ising model. This model requires the evaluation of the so-called pair interaction parameters, $J_{AB(n)}$, which operate at specific interatomic distances. These parameters can be evaluated only via an atomistic model.

As shown below, the $W_{AB}$ and $J_{AB(n)}$ parameters can be computed from excess enthalpies of supercells containing single and paired substitutional defects. In this study these calculations are performed with $2 \times 2 \times 2$ supercells of barite with the compositions of $AB_{31}(SO_4)_{32}$ and $A_2B_{30}(SO_4)_{32}$, where $A$ = Ba,Sr,Ra; $B$= Ba,Sr,Ra; $A \neq B$. In such a supercell, a single defect can be placed in any of the 32 equivalent positions, while a pair of defects can be inserted in 17 variants defined by the defect-defect distance. Thus, the derivation of $W_{AB}$ requires a single geometry optimization (energy minimization) calculation, while the derivation of all $J_{AB(n)}$ parameters requires a larger computational effort. Here, the $W_{AB}$ and $J_{AB(n)}$ parameters are evaluated both ab initio and with an empirically parameterized force-field model. The ab-initio total energies required for these evaluation were computed with the density functional theory (DFT) package CASTEP (Clark et al., 2005) using the Wu-Cohen density functional (Wu and Cohen, 2006). These calculations included optimizations of the electronic degrees of freedom, the atomic coordinates and unit-cell parameters. In all calculations the kinetic energy cutoff of the plane wave basis set was set at 1100 eV. The average distance between individual k-points was $\sim 0.03$ Å$^{-1}$. The effects of the core electrons on the wave functions of valence electrons were modelled with the ultrasoft on-the-fly-generated pseudopotentials supplied with the Materials Studio 7 software package [http://accelrys.com/products/collaborative-science/biovia-materials-studio]. Each geometry optimization required about 20000 CPU hours on the JuRoPa or JuReCa clusters at the Juelich Supercomputing Centre. The force-field static lattice energy minimization calculations were performed with the program GULP (Gale and Rohl, 2003). A geometry optimization task with GULP required about 0.5 min for each supercell on a single CPU. The calculations were performed with an empirical force-field model of Allan et al. (1993). The modifications relative to the original set of Allan et al. (1993) consisted in the parameterization of the Buckingham Ba – O interaction potential, $A \exp(-r/\rho)$, which was slightly adjusted to fit the unit cell parameters of barite from the study of Jacobsen et al. (1998). The new values are $A$ = 4131.96028 eV and $\rho$ = 0.290612 Å. Additionally, the Ra – O interaction potential with the parameters $A$ = 3835.82299 eV and $\rho$ = 0.299836 Å was introduced. The values for Ra – O were obtained by fitting to unit cell parameters of $RaSO_4$ from the study of Weigel and Trinkl (1973).

Below the binary regular mixing and the generalized Ising models are discussed in further details. The generalization of the binary models into their ternary variants follows this discussion.

#### 2.1.1. Regular mixing model

In an (A,B)$L$ solid solution in the dilute limit of $x_B \ll 1$, the insertion of a single substitutional defect B into an A-rich host causes the formation of $Z_n$ pairs of AB-type at the $n$-th distance from the B defect, where $Z_n$ is the coordination number within the $n$-th shell about the defect. The contribution to the enthalpy of mixing due to the formation of each AB pair is equal to a half of the enthalpy effect of the reaction AA + BB = 2AB, which is called the pair interaction energy or the pairwise interaction, $J_{AB(n)}$. In the dilute limit each B atom is surrounded by $Z_n$ A atoms with the probability of 1, therefore, the enthalpy of mixing per 1 mol of A and B atoms can be written as

$$H_{mix}(\text{dilute limit}) = x_B \frac{1}{2} \sum_{n=1}^{N} Z_n J_{AB(n)} = x_B W_{AB}, \quad (3)$$

where $W_{AB}$ is the regular interaction parameter, $x_B$ is the mole fraction of B defects and $N$ is the distance (order of neighbors) above which the pair interaction energy is thought to be negligible. Here $N$ is equal to 17. When the dilution limit is lifted, while the distribution of A and B atoms remains perfectly random, the probability of finding an A atom next to a given B atom reduces from 1 to $x_A$. Thus, Eqn. (3) is modified as follows

$$H_{mix}(\text{regular}) = x_A x_B W_{AB}. \quad (4)$$

The last equation is consistent with the regular mixing model (Hildebrand, 1929). The $W_{AB}$ parameter contains the total effect of the pairwise interactions at all distances. Their particular values are not important at this level of theory. We note, however, that typically the $J_{AB(n)}$ values vary with the composition. Under the assumption that this variation is linear

$$J_{AB(n)} = J_{AB/A(n)} x_A + J_{AB/B(n)} x_B, \quad (5)$$

where the values of $J_{AB/A(n)}$ and $J_{AB/B(n)}$ are defined in the limits of pure A$L$ and B$L$, respectively, Eqn. (4) transforms into the subregular form

$$H_{mix}(\text{subregular}) = x_A x_B (x_A W_{AB/B} + x_B W_{AB/A}). \quad (6)$$

The values of $W_{AB/A}$ and $W_{AB/B}$ are evaluated here with the Single Defect Method (SDM) (Sluiter and Kawazoe, 2002). The SDM is based on noting that $W_{AB/A}$ and $W_{AB/B}$ are equal to the slopes of the enthalpy of mixing function (Eqn. (6)) in the vicinity of pure phases A$L$ and B$L$. The slopes can be computed as the ratios of finite changes in the excess enthalpy and in the composition of a supercell of the host phase due to an insertion of a single substitutional defect corresponding to the other end member. The change in the mole fraction is given by the defect/host ratio, i.e. by the inverse of the number of the exchangeable sites, $m$, in the supercell. Therefore,

$$W_{AB/A} \approx \left.\frac{dH_{mix}}{dx_B}\right|_{x_B=0} \approx \frac{\Delta H_{mix}(\text{at } x_B = 1/m)}{1/m} = \Delta H_B. \quad (7)$$

Similarly, $W_{AB/B} = \Delta H_A$. In this study $m$ = 32.

Although the obtained parameters are valid only in the dilute limits, they usually perform well in the high-temperature limit too. This can be verified by computing directly the excess energy of a supercell, in which the distribution of A and B is randomized. A supercell with a nearly perfectly random distribution can be emulated with the help of a special quasi-random structure (QRS). A QRS is an ordered structure (i.e. a supercell with a certain A,B arrangement over the $m$ sites) with well-defined cluster frequencies (Zunger et al., 1990), whose enthalpy provides the best estimate of the average enthalpy of a disordered solution. Here such a QRS has been chosen from a large set of randomly modified supercell structures according to the criteria that the normalized frequencies of AB-type pairs at each distance within a $2 \times 2 \times 2$ supercell deviate negligibly from $^1/_2 x_A x_B Z_n$. The Margules parameter $W_{AB}$ ($W_{AB} = (W_{AB/A} + W_{AB/B})/2$) is equal to four times the excess enthalpy of a QRS structure with $x_A = x_B = 0.5$, when the excess quantity is counted per mole of cations. If the excess enthalpy of the QRS falls onto the enthalpy of mixing function defined by Eqn. (7), this means that the $W_{AB/A}$ and $W_{AB/B}$, calculated with the SDM perform well non only in dilute limits, but also in the high-temperature limit.

#### 2.1.2. Generalized Ising model

SDM and QRS methods evaluate the combined effects of pairwise interactions in a disordered solution. Although the $W_{AB}$ value can be efficiently computed, a perfectly random distribution of A and B can hold only at dilute or high-temperature limits. At intermediate compositions and moderate temperatures, various effects of ordering alter the pair probabilities, thus making the regular model inaccurate. In a real solid solution, the probability of finding an AB pair at a given

distance, $p_{AB(n)}$, can significantly deviate from $x_A x_B$. Such deviations are referred to as short-range ordering (SRO). SRO is caused by differences in values of the $J_{AB(n)}$ parameters. Typically, $J_{AB(n)}$ vary as a function of $n$ in sign and in magnitude, reflecting the relative ease or difficulty of creating defects at given distances and directions within a given structure. If $J_{AB(n)}$ is negative for a given $n$, $p_{AB(n)}$ will increase over the $x_A x_B$ value, while if $J_{AB(n)}$ is positive, $p_{AB(n)}$ will decrease. These deviations are typically magnified at $x_B = 0.5$, where the relative fractions of AB pairs increase. As these deviations are counterbalanced by the entropy factor, $p_{AB(n)}$ are also functions of the temperature. To allow for a variation in $p_{AB(n)}$, the enthalpy of mixing is modelled with the equation

$$H_{mix}(\text{Ising}) = \frac{1}{2}\sum_{n=1}^{N} p_{AB(n)} Z_n J_{AB(n)}. \tag{8}$$

If the $J_{AB(n)}$ are known, the values of $p_{AB(n)}$ and $H_{mix}$ can be determined with the Monte Carlo method (e.g. Warren et al., 2001).

A computationally convenient algorithm for the determination of $J_n$ is offered by the Double Defect Method (DDM) (e.g. Hoshino et al. (1993), Vinograd et al. (2009, 2010), Liu et al. (2016)). It has been shown that a $J_{AB(n)}$ is a function of the excess enthalpy of a supercell structure prepared from an end-member AR by the insertion of a pair of B defects at the $n$-th distance from each other. Namely,

$$J_{AB/A(n)} = (2\Delta H_B - \Delta H_{BB(n)})/D_n \tag{9}$$

where $D_n$ is the degeneracy factor, which counts the number of BB pairs created per single B defect due to the periodic boundary conditions applied to the supercell. This number is typically 1 for pairs located at short distances, however, it takes larger integer values ($1 \le D_n \le Z_n$) for pairs whose distances approach half of the body diagonal of the supercell. The $D_n$ and $Z_n$ values for a $2 \times 2 \times 2$ supercell are given in Table A1 in Appendix A3. The pairwise interactions in the B-rich limit are computed similarly via

$$J_{AB/B(n)} = (2\Delta H_A - \Delta H_{AA(n)})/D_n \tag{10}$$

where $\Delta H_A$ and $\Delta H_{AA(n)}$ are the excess enthalpies of supercell structures of the host B with single, A-type, and double, AA-type, substitutional defects. Importantly, $\Delta H_B$ and $\Delta H_A$ must satisfy

$$\Delta H_B = W_{AB/A} = \frac{1}{2}\sum_{n=1}^{N} Z_n J_{AB/A(n)} = \frac{1}{2}\sum_{n=1}^{N} Z_n (2\Delta H_B - \Delta H_{BB(n)})/D_n \tag{11}$$

and

$$\Delta H_A = W_{AB/B} = \frac{1}{2}\sum_{n=1}^{N} Z_n J_{AB/B(n)} = \frac{1}{2}\sum_{n=1}^{N} Z_n (2\Delta H_A - \Delta H_{AA(n)})/D_n. \tag{12}$$

Eqns. (11) and (12) are often slightly violated due to computational inaccuracies, but the equalities can always be restored via slight adjustments in the values of $\Delta H_B$ and $\Delta H_A$. These adjusted values are actually used to compute the pairwise interactions via Eqns. (9) and (10), thus ensuring consistency between the $J_{AB/(n)}$ and $W_{AB}$ parameters. This consistency means that the enthalpy of mixing computed with Eqn. (8) would converge to the subregular mixing model when the pairwise probabilities approach the value of $x_A x_B$. This behaviour is seen in Monte Carlo results obtained at a very high temperature.

### 2.1.3. Modelling of mixing in a ternary regular solid solution

The regular mixing model introduced above can be extended to a ternary system via the equation of Wohl (1946) (see also Ganguly, 2001)

$$H_{mix} = \sum_{I \ne J}^{N} x_I x_J W_{IJ} + x_I x_J x_K W_{IJK}, \tag{13}$$

where $W_{IJ}$ are the binary mixing parameters and the $x_I$ are ternary mole fractions. Eqn. (13) contains a ternary parameter. The need for this parameter is specially investigated in Appendix A2. When $W_{IJK} = 0$ the ternary interactions are absent and the excess enthalpy is obtained by combining the $W_{IJ}$ parameters defined in the binaries. The entropy of mixing is modelled with the familiar equation implying the complete randomness

$$S_{mix} = -R\sum_{I} x_I \ln x_I, \tag{14}$$

while the ternary Gibbs energy of mixing is computed as

$$G_{mix} = H_{mix} - TS_{mix}. \tag{15}$$

### 2.1.4. The ternary Ising model

The generalized Ising model can be extended to the ternary system as follows

$$H_{mix} = \frac{1}{2}\sum_{I \ne J}\sum_{n=1}^{N} p_{IJ(n)} Z_n J_{IJ(n)}, \tag{16}$$

where the first summation is over the three different types of pairs, AB, AC, and BC. The problem is that the dependence of $J_{IJ(n)}$ on the ternary composition should be specified. As the first approximation, a linear dependence of $J_{IJ(n)}$ on the ternary mole fractions can be assumed:

$$J_{IJ(n)} = J_{IJ/I(n)} x_I + J_{IJ/J(n)} x_J + J_{IJ/K(n)} x_K \tag{17}$$

The first two summands in Eqn. (17) contain the familiar binary $J_{IJ(n)}$ parameters, which are computed with the DDM. The last term defines the dependence of the $J_{IJ(n)}$ on the third component $K$. This parameter can be computed with a ternary variant of the DDM (Vinograd et al., 2010), in which the excess effects are computed for IJ-, II- and JJ-type double-defect structures inserted into a supercell of pure KR composition. Our ab initio calculations along this approach were not fully successful, resulting in unreasonably large fluctuations in the values $J_{IJ/K(n)}$. However, our force-field calculations, suggested that the $J_{IJ/K(n)}$ interactions can be reasonably accurately predicted with the approximation

$$J_{IJ/K(n)} = (J_{IJ/I(n)} x_I + J_{IJ/J(n)} x_J)/(x_I + x_J), \tag{18}$$

This approximation is further used in this study. Eqn. (18) can be shown to be consistent with Eqn. (13) under the assumption of $W_{IJK} = 0$. On the contrary, a deviation from Eqn. (18) would imply the existence of specific ternary interactions. A good performance of Eqn. (13) in predicting the enthalpies of ternary QRS under the condition of $W_{IJK} = 0$ (see Appendix A2) can be viewed as a proof for the validity of the approximation implied in Eqn. (18).

### 2.1.5. Calculation of free energies of mixing

The excess energy of a supercell structure with a given arrangement of A, B and C cations can be computed with Eqn. (16), in which the probabilities of AB, AC and BC pairs are interpreted as the normalized occurrence frequencies. The dependence of $\Delta H_{mix}$ on the temperature is modelled here with Monte Carlo simulations. Each simulation consisted in generating a sequence of $2{\cdot}10^7$ configurations starting with an $8 \times 12 \times 8$ supercell (3072 lattice sites) with known (fixed) A/(A + B + C) and B/(A + B + C) ratios. The sequence was produced by swapping randomly chosen AB, BC and AC pairs, where the swap acceptance/rejection probability was defined via the Metropolis algorithm (Metropolis et al., 1953). The tail of the sequence composed of $10^7$ configurations was assumed to converge to the Boltzmann probability distribution. The temperature dependent enthalpy was computed by a simple averaging of enthalpies of the converged tail of configurations. At each given temperature and composition, simulations were repeated at different values of the λ-parameter, $0 < \lambda < 1$, which was used to define the degree of randomness of pairwise interactions via $J_\lambda = \lambda J$. The Gibbs energy of mixing was obtained via the equation

$$\Delta G_{mix} = \Delta G^{0}_{mix} + \int_{\lambda=0}^{\lambda=1} \Delta H^{\lambda}_{mix} d\lambda, \quad (19)$$

where $\Delta G^{0}_{mix}$ is the Gibbs energy of mixing of a solid solution at a given temperature and composition constrained to have completely random pairwise probabilities. Effectively, $\Delta G^{0}_{mix}$ corresponds to the free energy of the binary or ternary regular mixing in the system, while the integral evaluates the free energy deviations due to short- and long-range ordering. The step in the λ parameter was set equal to 0.04. Steps in mole fractions and in the temperature were 0.03125 and 50 K, respectively; the temperature varied from 598 to 98 K. Isosurfaces of the Gibbs energy of mixing were computed over a grid of 561 ternary compositions.

#### 2.1.6. Representation of the free energies of mixing

Obviously, the digital character of the obtained Gibbs energies poses a problem in applying them for calculating thermodynamic equilibrium in chemically complex systems. Indeed, the currently available software tools, e.g. GEM Selector (Kulik et al., 2013) require the Gibbs energy to be expressed as a differentiable function of the composition. This implies that the Gibbs free energy grid obtained from a Monte Carlo simulation must be fitted into a mathematically suitable form. In this study, this was achieved via the ternary regular mixing model, in which the enthalpy of mixing was modelled via Eqn. (13), while the interaction parameters were adjusted to the Monte Carlo results such that the shape of the ternary miscibility gap was closely reproduced. Although such a fit can be performed via an automatized routine, here it was performed via a manual variation of the binary $W_{ij}$ parameters. Indeed, we noted that the shape of the miscibility gap in the ternary system is mostly sensitive to the value of $W_{BaSr}$. The optimal set $W_{ij}$ values, which best fits the Monte Carlo results could be relatively easily found via a very limited set of regular model calculations consisting of two steps. At the first step, the value of $W_{BaSr}$ was varied within the interval of 4–9 kJ/mol with a step of 0.05 kJ/mol, while the $W_{BaRa}$ and $W_{SrRa}$ were fixed at the values predicted via the SDM calculations. At the second step the values of $W_{BaSr}$ and $W_{BaRa}$ were fixed and the value of $W_{SrRa}$ was varied. The ternary miscibility gap was visualized by constructing a convex hull and by projecting it onto the ternary composition diagram, as described by Vinograd et al. (2010). In the convex hull algorithm, each point of the original free energy surface is substituted by a combination of three points corresponding to the energies that give the lowest energy value for the same average composition. A concave area is thus substituted by a triangle of the minimal size that is defined by the grid density. Miscibility gaps can thus be visualized as agglomerations of large thin triangles elongated along tie-lines, while miscible regions are seen as agglomerations of isometric triangles of minimum area.

### 2.2. Celestite recrystallization in the presence of a Ra-bearing aqueous solution

#### 2.2.1. Sample preparation and experimental setup

The general batch experimental setup was adapted from earlier studies on barite recrystallization (e.g. Brandt et al., 2015; Klinkenberg et al., 2014). A high purity celestite (99.99+ %), as purchased from Chempur®, was put into contact with a Ra-tracer at room temperature and the uptake of Ra was observed, starting from a Ra-concentration of $5.0 \cdot 10^{-6}$ moL/L and 0.1 moL/L of NaCl as background electrolyte. The Chempur® celestite is characterized by particles in the grain size range between 0.5 and 5 μm. A parallel Ra-free reference experiment was carried out in order to compare the Sr and Ba concentrations released from celestite in the presence and absence of Ra as a function of time. In addition, a blank experiment without solid was carried out to evaluate the adsorption of Ra on the glass bottles. An overview of all experiments is given in Table 1.

**Table 1**
Overview of experiments in 0.1 moL/L NaCl at room temperature.

| Name | Solid/Liquid | Initial Ra concentration | Duration of the experiment |
|---|---|---|---|
| | (g/L) | ($10^{-6}$ mo/L) | (days) |
| Blank Ra | – | 5 | 443 |
| Reference 0.5 g/L SrSO4_RT | 0.5 | 0 | 828 |
| 0.5 g/L SrSO4_RT | 0.5 | 5 | 828 |

#### 2.2.2. Sampling and analyses of the aqueous solution

The sampling procedure was the same as in Klinkenberg et al. (2014), i.e. 500 μL of the aqueous solution were taken at regular time intervals and directly filtered after a settling time of 1 h through Advantec ultrafilters (MWCO = 10,000 Da). The Ra concentration in solution was quantified via Gamma spectrometry using a $N_2$ cooled high purity Ge-detector. The intensity of the Ra peak at 186 keV was determined using Gamma-W for Windows (Version 2.55, Interaktive Spektrum Analyse, Dr. Westmeier, Gesellschaft für Kernspektrometrie mbH) and converted to a concentration (mol/L). The system was calibrated with an independent, external standard. The Sr and Ba concentrations in solution were quantified using an ICP-MS ELAN 6100 DRC (PerkinElmer SCIEX) instrument. The filtered solution was diluted in 0.1 m $HNO_3$.

#### 2.2.3. Analysis of the solids: scanning electron microscopy (SEM) and energy dispersive x-ray spectrometry (EDS)

Small amounts of solid were sampled during the recrystallization experiments. The evolution of the crystals morphology and chemical composition was studied using the environmental scanning electron microscope FEI Quanta 200 FEG combined with energy dispersive x-ray spetcrometry (EDS, EDAX). In order to avoid artifacts due to precipitation of NaCl, $SrSO_4$ or $RaSO_4$, the samples were separated from their solution by two washing steps in iso-propanol. The samples were then prepared as a suspension on a Cu holder and subsequently dried.

### 2.3. GEM-selector thermodynamic modelling

SS-AS equilibria were modelled with the GEM-Selektor code package (Kulik et al., 2013; http://gems.web.psi.ch) that includes the TSolMod library of models of mixing (Wagner et al., 2012) and the GEMS version of PSI-Nagra 12/07 chemical thermodynamic database (Hummel et al., 2002; Thoenen et al., 2014). In GEM-Selektor, the phase equilibrium is found via direct minimization of the total Gibbs energy of the system defined by its bulk elemental composition, temperature, pressure, standard Gibbs energy per mole of all chemical species, and parameters of mixing in phases-solutions. Thermodynamic data for solid sulfates (Table 2) and for aqueous species are taken from the GEMS version of the PSI-Nagra database (Thoenen et al., 2014) that inherits temperature and pressure dependencies from the HKF EoS data for most aqueous ions and complexes as well as the HGK EoS for the water-solvent (Helgeson et al., 1981) as given in the SUPCRT98 database. The built-in ternary regular model (Wagner et al., 2012) is used to describe the thermodynamics of mixing in the ternary. For aqueous species, the aqueous electrolyte ion association model consistent with

**Table 2**
Thermodynamic data for sulphate end members used in GEM calculations.

| Solid | $\log K^{o}_{s298}$ | $\Delta_r G^{o}_{298}$ | $G^{o}_{298}$ |
|---|---|---|---|
| $SrSO_4$ | −6.63 | 37.84 | −1346.14 |
| $BaSO_4$ | −9.97 | 56.91 | −1362.15 |
| $RaSO_4$ | −10.26 | 58.56 | −1364.52 |

All values at 1 bar, 25 °C. Units: kJ/mol; logK for reactions: $MSO_4 = M^{2+} + SO_4^{2-}$.

the SUPCRT92 database and the built-in extended Debye Hueckel model (Johnson et al., 1992) was used.

The typical input recipe for a system contained 1 kg of water, 0.1 mol of NaCl, 0.5 (or 5) grams of $BaSO_4$, $5.0{\cdot}10^{-6}$ mol of $RaCl_2$, and $1.0{\cdot}10^{-6}$ mol $O_2$. Calculations were performed at $T$ = 23 °C or 25 °C and $P$ = 1 bar.

A complete thermodynamic dataset for the system (Ba,Sr,Ra) $SO_4 + H_2O$ in GEMS and PHREEQC forms that includes the temperature dependence of $RaSO_4$ solubility is discussed in a companion paper (Vinograd et al., 2017).

## 3. Results

### 3.1. Thermodynamics of mixing in the ternary system

#### 3.1.1. Parameterization of the regular model of mixing

The results of calculations based on the single defect method (SDM) have been already reported for some of the binary systems within the barite family (Vinograd et al., 2013). In this study, these calculations are repeated with a better precision and the results are extended to all possible combinations of the host-solute pairs to give a complete set of the subregular model parameters for (Ba,Sr,Ra)$SO_4$ solid solution. Here we also demonstrate the consistency between values of regular mixing parameters computed with the single-defect method and those obtained with the aid of quasi-random structures (QRS). The binary $W_{IJ/J}$, $W_{IJ/I}$ and $W_{IJ}$ parameters computed with the SDM are given in Tables 3 and 4. Table 3 gives the values computed with the DFT-based CASTEP code, while Table 4 lists the analogous values computed from the modified force-field model of Allan et al. (1993). Fig. 1 shows the enthalpy of mixing functions of the binary (Ba,Ra)$SO_4$, (Ba,Sr)$SO_4$ and (Sr,Ra)$SO_4$ systems computed ab initio with the SDM. The Sr-Ra and Ba-Ra binaries are characterized by the largest and the smallest enthalpies of mixing, respectively. This is consistent with the observation that the excess effect is proportional to the squared volume difference between the end-members (Vinograd et al., 2013; Kowalski and Li, 2016). The results obtained with quasi-random structures (QRS) are also shown in Fig. 1 and given in Table 3. Obviously, the enthalpies of the QRS are consistent with the SDM results. The differences between these two sets of values can be interpreted as the uncertainties of the derived parameters. This uncertainty does not include systematic errors inherent to the functional and the pseudopotentials used in the DFT calculations. We assume that the latter errors should not exceed the differences between the $W$ values given in Tables 3 and 4 The total uncertainty is taken as the sum of the two differences. The SDM DFT-based average values are taken as the final result. The values $W_{BaRa}$ = 2.47 ± 0.22, $W_{BaSr}$ = 8.34 ± 0.75 and $W_{SrRa}$ = 19.80 ± 1.40 kJ/mol were used to compute the Gibbs free energy of the ternary regular solid solution (see Section 3.1.2).

#### 3.1.2. Ternary regular model

Fig. 2 shows the convex-hull analysis of the Gibbs free energy surface which corresponds to the ternary regular model with the $W_{ij}$ parameters from Table 3 (the average SDM values). The miscible convex areas are seen as agglomerations of small triangles, while the miscibility gaps appear as agglomerations of elongated triangles.

**Table 3**
Binary Margules parameters (kJ/mol) computed with DFT from excess energies of the single-defect and QR structures.

| Subregular model (SDM) | | | | Regular model (Average of the subregular parameters) | | Regular model (QRS) | |
|---|---|---|---|---|---|---|---|
| $W_{BaRa/Ba}$ | 2.63 | $W_{BaRa/Ra}$ | 2.31 | $W_{BaRa}$ | 2.47 | $W_{BaRa}$ | 2.48 |
| $W_{BaSr/Sr}$ | 7.75 | $W_{BaSr/Ba}$ | 8.92 | $W_{BaSr}$ | 8.34 | $W_{BaSr}$ | 8.54 |
| $W_{SrRa/Sr}$ | 20.31 | $W_{SrRa/Ra}$ | 19.30 | $W_{SrRa}$ | 19.80 | $W_{SrRa}$ | 18.56 |

**Table 4**
Binary Margules parameters (kJ/mol) computed with the force-field model from excess energies of the single-defect and QR structures.

| Subregular model (SDM) | | | | Regular model (Average of the subregular parameters) | | Regular model (QRS) | |
|---|---|---|---|---|---|---|---|
| $W_{BaRa/Ra}$ | 2.22 | $W_{BaRa/Ba}$ | 2.29 | $W_{BaRa}$ | 2.26 | $W_{BaRa}$ | 2.35 |
| $W_{BaSr/Sr}$ | 9.01 | $W_{BaSr/Ba}$ | 8.78 | $W_{BaSr}$ | 8.89 | $W_{BaSr}$ | 9.01 |
| $W_{SrRa/Ra}$ | 19.29 | $W_{SrRa/Sr}$ | 20.63 | $W_{SrRa}$ | 19.96 | $W_{SrRa}$ | 20.00 |

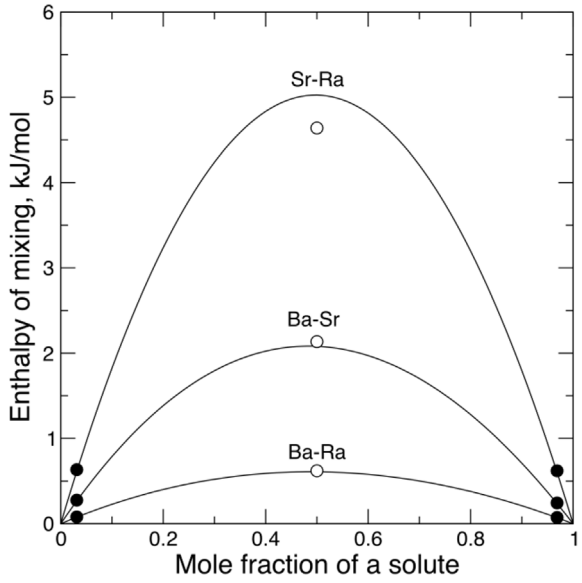


**Fig. 1.** Enthalpies of mixing in binary systems computed with the single defect method. Solid lines correspond to the subregular model, where the Margules parameters are given in Table 3. The solid circles in the dilute limits are the excess enthalpies of the single-defect supercell structures per one $SO_4$ unit. The open circles at intermediate compositions are the excess enthalpies of quasi-random structures scaled per one $SO_4$ unit.

Importantly, the elongations of these triangles approximately follow the tie-lines. The model predicts a large miscibility gap within the ternary. At ambient temperatures, the miscibility is restricted to two composition domains, the Ba,Ra-rich, Sr-poor phase, in which complete mixing is observed at all temperatures above 198 K, and the Sr,Ba-rich, Ra-poor phase, whose composition extends towards $BaSO_4$ at $T$ > 500 K. In the (Ba,Sr)$SO_4$ binary, the miscibility gap closes at about 500 K, while in the (Sr,Ra)$SO_4$ system it is present up to ~1200 K. The predicted value of $W_{BaSr}$ of 8.3 kJ/mol that causes the gap closing above 500 K appears to contradict to observations from natural samples (e.g. Lerouge et al., 2014), which suggest that full miscibility exists in this system at diagenetic conditions (300 < $T$ < 400 K). Consistently with this observation, Heberling et al. (2017) have recently reported on a wide range of Ba/Sr ratios in (Ba,Sr)$SO_4$ scales crystallized at ~343 K in pipes of a hydrothermal power plant. No indications to the existence of a miscibility gap at these conditions have been found. We show below that the value of the effective $W_{BaSr}$ parameter is decreased significantly when short-range ordering is taken into account via the generalized Ising model.

#### 3.1.3. Pairwise interactions and the effects of ordering

The binary systems were further investigated with the generalized Ising model. Fig. 3 (left) shows the excess enthalpies of 2 × 2 × 2 supercells of barite with RaRa and SrSr defects, and with SrSr defects in $RaSO_4$. The pairwise interactions, i.e. the energies of the exchange reactions AA + BB = 2AB, where A,B = {Ba, Ra, Sr}, are trivially extracted from the excess enthalpies via the Double Defect Method (Vinograd et al., 2009). The pairwise interactions are plotted in Fig. 3

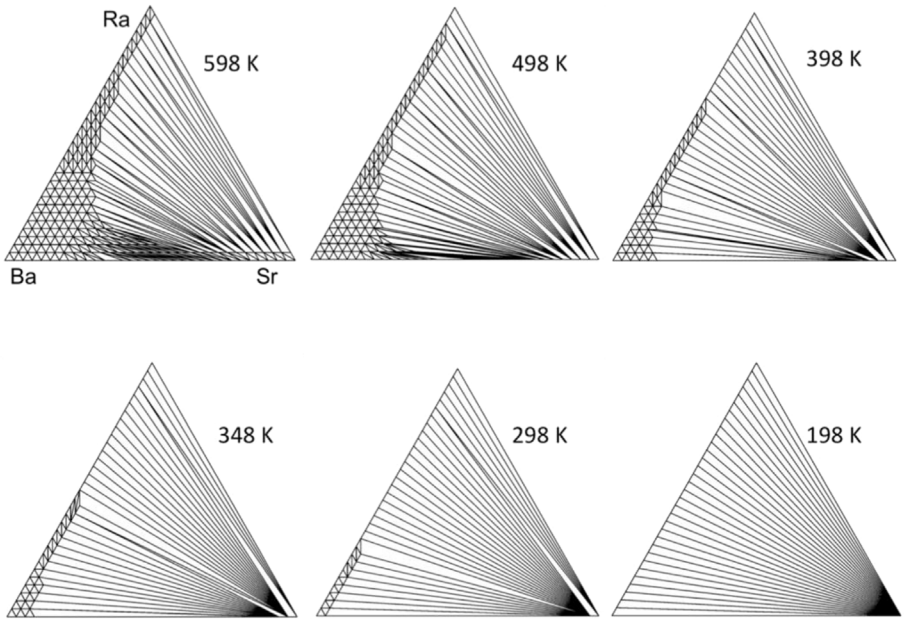


**Fig. 2.** Convex-hull projections of the Gibbs free energy surfaces computed with the ternary regular mixing model using the binary interaction parameters predicted with DFT. The grid is defined by the minimum equilateral triangle with the edge of $l/32$, where $l$ is the length of the edge of the largest triangle. The regions of miscibility are seen as agglomerations of triangles with areas of the minimal size.

(right). The patterns of the energy change vs. distance are very similar in all three systems. The magnitude of the pairwise interactions increases consistently with the volume mismatch between end-members.

The effect of composition on the pairwise interactions was further investigated with DFT for (Ba,Ra)$SO_4$ and (Ba,Sr)$SO_4$ systems. Fig. 4 (left) compares the excess energies of RaRa defects in a barite host to the excess energies of BaBa defects in a $RaSO_4$ host. The insertion of RaRa pairs into the barite host causes slightly larger excess energies. This is consistent with the usually observed stronger increase in the energy upon an insertion of a larger cation, which is related to a more rapid increase of the interaction energy of two ions upon a contraction rather than on an extension (Dove, 1993). The patterns of energy change vs. the defect-defect separation are very similar in the two sets. This shows that BaRa interactions, i.e. the energies of reactions BaBa + RaRa = 2BaRa, are approximately independent of the composition of the binary system. The whole set of data on (Ba,Ra)$SO_4$ thus confirms the previous result (Vinograd et al., 2013) that the mixing in this system can be well described with a regular model with the $W$ parameter in the range of 2.3–2.6 kJ/mol. The average value of 2.47 kJ/mol obtained from Ba and Ra defects in $RaSO_4$ and $BaSO_4$, respectively, is adopted for further modelling studies.

A rather different picture is seen in the case of BaSr interactions. The excess enthalpies of BaBa defects in the $SrSO_4$ host on average are smaller than the analogous values for SrSr defects in $BaSO_4$ (Fig. 4, right).

This observation is consistent with the SDM result (Table 3), which shows that the insertion of a single $Ba^{2+}$ into $SrSO_4$ costs less energy that the insertion of a single $Sr^{2+}$ into $BaSO_4$. This causes $W_{BaSr/Sr}$ to be smaller than $W_{BaSr/Ba}$. We note also that the excess energies of structures with BaBa defects placed at the third-, fifths- and sixths-neighbour distances are markedly smaller than the energies of the other structures (Fig. 4, right). These structures appeared to be not stable within the barite symmetry. A similar problem occurred with supercell structures containing RaRa defects in the celestite host. The origin of this anomalous behaviour is explained in Appendix A1. Therefore, in the present study, the BaSr and RaSr pairwise interactions were computed only from SrSr-defect structures built from the $BaSO_4$ and $RaSO_4$ hosts, respectively. The effects of composition on pairwise interactions were estimated based on the difference in the excess energies of the single-defect structures. Therefore, the values of $J_{BaSr/Sr}$ were scaled relative to the values of $J_{BaSr/Ba}$ by a factor of 0.87, while the values of $J_{SrRa/Sr}$ were scaled by a factor of 1.052 relative to the values of $J_{SrRa/Ra}$. This scaling ensured the consistency between DDM and SDM results. On the other hand, the absence of a strong asymmetry in binary $W$ parameters

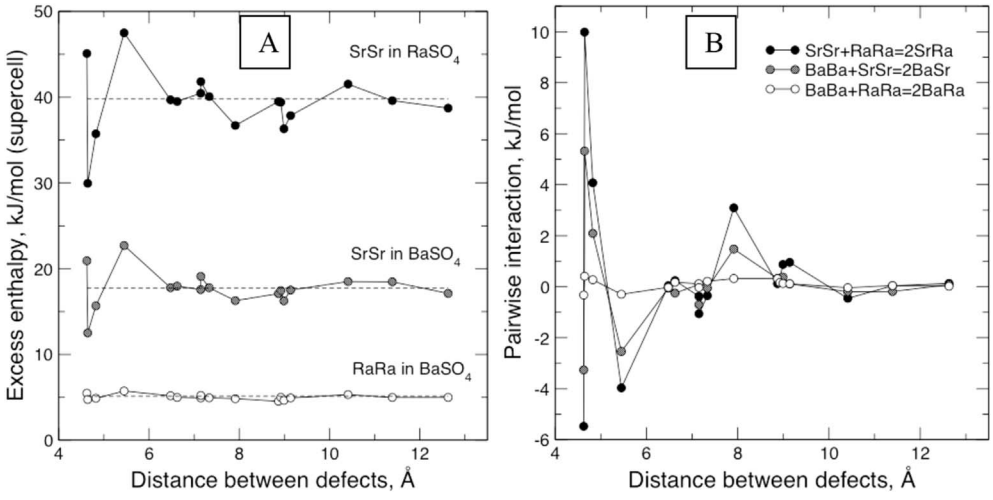


**Fig. 3.** Left: Excess energies of 2 × 2 × 2 supercells of $BaSO_4$ and $RaSO_4$ with different types of paired defects. The dashed lines correspond to twice the excess enthalpy of the single-defect structures. Right: Pairwise interactions computed from the excess energies with the DDM. Excess energies are computed with DFT.

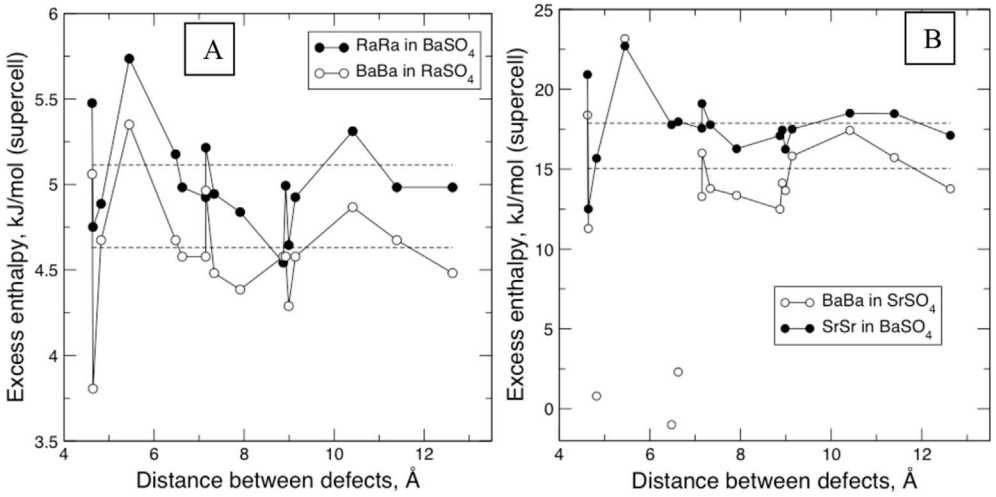


**Fig. 4.** Excess enthalpies of 2 × 2 × 2 barite-type structures with paired defects plotted against the defect-defect distance. Left: RaRa defects in $BaSO_4$ and BaBa defects in $RaSO_4$. Right: SrSr defects in $BaSO_4$ and BaBa defects in $SrSO_4$. The structures with BaBa defects at the third, fifth and sixth distances show anomalously low excess enthalpies. These structures adopt an unusual relaxation mechanism, which involves a wavy rotation of the $SO_4$ tetrahedra. The excess energies are computed with DFT.

(Tables 3 and 4) justifies the assumption that there should be no strong asymmetry in the pairwise binary interactions. This implies that the DFT-based interaction energies, which are computed only for Ba-rich and Ra-rich compositions, could be used to model the whole ternary composition space. The set of the pairwise interactions is given in Appendix A3. These interactions were used to define the mixing energy in the ternary Monte Carlo Ising model.

### 3.1.4. The generalized Ising ternary model

Table A2 in Appendix A3 lists the pairwise interaction energies, which were used to simulate the ternary mixing. A distinction between the phase relations predicted based on the regular mixing and the generalized Ising model is primarily seen in the $(Ba,Sr)SO_4$ binary. In the generalized Ising model, the Ba-Sr miscibility gap occurs at a much lower temperature. Particularly, the regular model predicts the closing of the miscibility gap at about 500 K, while in the Ising model, the closing occurs at about 280 K. The stabilization of the disordered phase relative to the mixture of the end-members is due to short-range ordering (SRO). The SRO effect is best seen in the enthalpy vs. composition plot as a significant decrease in the enthalpy of mixing at ambient temperatures (Fig. 5). The systems of $(Ba,Ra)SO_4$ and $(Sr,Ra)SO_4$ are much less sensitive to a similar ordering. In the former case, the pairwise interactions are very weak. The phase separation occurs below

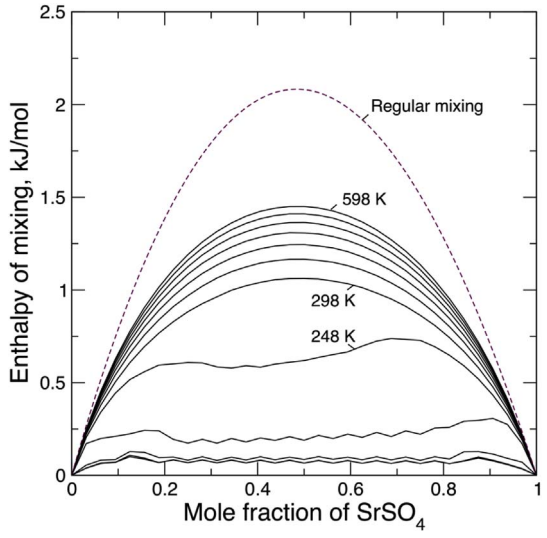


**Fig. 5.** The enthalpy of mixing isotherms in the $(Ba,Sr)SO_4$ solid solution computed with the Monte Carlo method. Dashed line corresponds to the subregular model with the parameters $W_{BaSr/Ba}$ = 8.92 and $W_{BaSr/Sr}$ = 7.75 kJ/mol.

150 K, i.e. at the temperatures, which are not particularly interesting for the present study. At ambient temperatures, the solid solution is essentially disordered. In the case of $(Sr,Ra)SO_4$, on the contrary, the pairwise interactions are strong and their total excess effect is so large that the solid solution decomposes at all temperatures of interest. Thus, at ambient temperatures the solid solution exists in the dilute limits only, where the regular mixing model remains valid. This implies that the $(Ba,Ra)SO_4$ and the $(Sr,Ra)SO_4$ solid solutions can be adequately modelled via the regular mixing model, while a SRO correction is required only in the $(Ba,Sr)SO_4$ binary.

Fig. 6 shows the convex-hull analysis of the free energy surfaces computed via the thermodynamic integration of the Monte Carlo results.

The effect of the SRO on the free energy of the solid solution can be emulated with the help of the regular mixing model by decreasing the $W_{BaSr}$ parameter to ~4.95 kJ/mol such that the miscibility gap closes at ~280 K as in the DDM-Monte-Carlo modelling. A small decrease in the $W_{SrRa}$ parameter relative to the SDM value also helps to approach the shape of the ternary miscibility gap produced using the Ising model. Thus, the set of parameters ($W_{BaRa}$ = 2.47 ± 0.22, $W_{BaSr}$ = 4.95 ± 0.75 and $W_{SrRa}$ = 17.50 ± 1.40 kJ/mol) together with the regular model equations can be used to emulate the phase relations computed with the rather tedious Monte Carlo simulations. Here, we would like to mention that the fit to the simulated ternary phase relations could be further improved, for example, by introducing asymmetry in the regular expressions for the binary systems. Our atomistic simulations show, however, that mixing in the binary systems is very close to be symmetric. Thus we decided not to introduce any further complexities into the ternary model. Although, we need to note that the regular description in principle cannot fully reflect the rather complex shape of the free energy surface obtained via the simulations over a wide temperature interval. The recommended set of the Margules parameter has been set to fit accurate only the interval of 298–398 K, which is of particular interest for safety assessments of nuclear waste repositories.

## 3.2. Phase relations in the system of $(Ba,Sr,Ra)SO_4 + H_2O$: thermodynamic modelling

### 3.2.1. The effect of Sr/Ba ratio on trace Ra uptake in ternary solid solution

The modelling aimed at assessing the effect of a variable content of $SrSO_4$ in Ba-sulphate solid solution at 23–25 °C at S/W ratios of 0.5 and 5.0 g/(kg $H_2O$) and at constant loading of $5.0{\cdot}10^{-6}$ molal $RaCl_2$. The composition of the solid solution was varied via a stepwise addition of $SrSO_4$ (starting from $1.0{\cdot}10^{-6}$ mol of $SrSO_4$) to the system bulk composition and by subtraction of $BaSO_4$ such that the mass of the solid

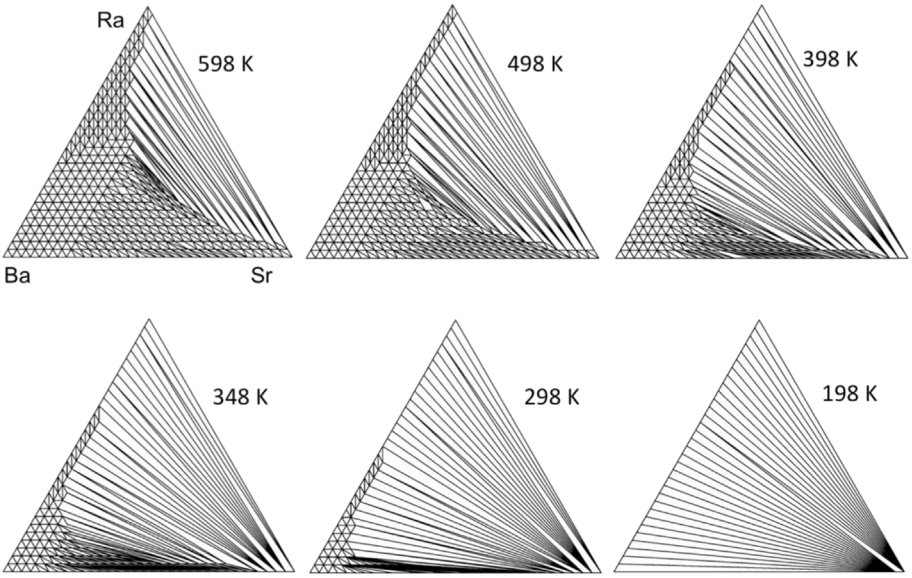


**Fig. 6.** Convex-hull projections of the Gibbs free energy surface of the (Ba,Sr,Ra)$SO_4$ solid solution in the range of 598–198 K. The free energy is from the Monte Carlo simulations, which are based on the generalized Ising model.

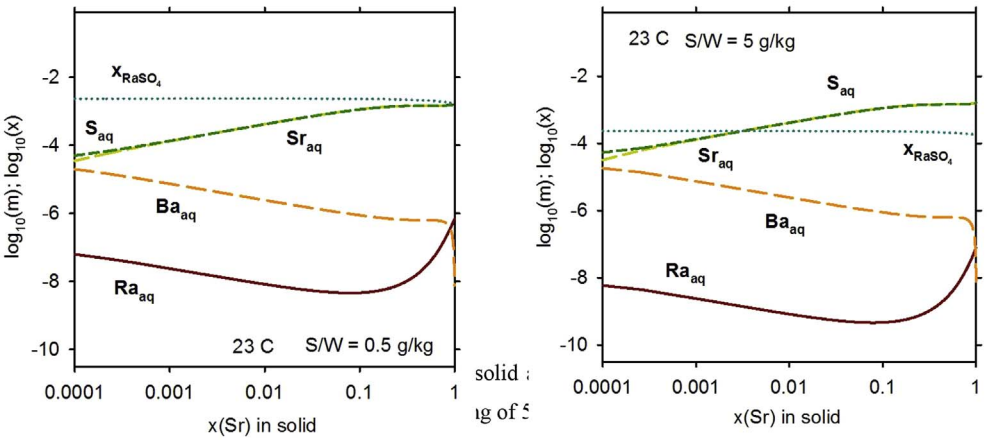


**Fig. 7.** Dependencies of the Ra contents in the solid and aqueous phases at 23 °C at 1 bar on the mole fraction of Sr in the solid phase at trace Ra loading of $5{\cdot}10^{-6}$ m and S/W = 0.5 (A) and 5.0 g/(kg $H_2O$) (B).

solution phase remained constant. The results of the simulations (Fig. 7) show that at Ba-rich compositions, the equilibrium aqueous concentration of Ra decreases as a function of the mole fraction of $SrSO_4$ in the solid, such that a clear minimum is observed at ~10 mol % $SrSO_4$.

This implies that the immobilization of Ra in the ternary (Ba,Sr,Ra)$SO_4$ solid solution at $x(SrSO_4) \sim 0.1$ is much more efficient than in the binary (Ba,Ra)$SO_4$ solid solution. On the other hand, at higher $x(SrSO_4)$, particularly above 0.5, the immobilization of trace Ra is predicted to be less efficient than in the (Ba,Ra)$SO_4$ solid solution. The retention of Ra in the solid is more efficient at the higher S/W of 5.0 g/(kg $H_2O$). Fig. 7 shows that Ra,aq concentrations are ca. 10 times higher at S/W = 0.5 g/(kg $H_2O$).

### 3.2.2. Modelling of the effect of Sr/Ba ratio on Ra uptake in the case of a phase separation

Although at trace Ra-concentration, the (Ba,Sr)$SO_4$ solution is predicted to be completely miscible at room temperature, at slightly elevated Ra-concentrations, the system composition would fall into the ternary miscibility gap. Our simulations suggest that an admixture of $RaSO_4$ causes the solid solution to separate into a Sr-rich phase and a phase, which is simultaneously rich in Ba and Ra. To simulate such a decomposition with GEM-Selektor, two ternary (Ba,Sr,Ra)$SO_4$ solid solutions (with identical mixing models) were included into the set of possible phases. The phase separation can be nicely illustrated with the system composition of $1{\cdot}10^{-5}$ mol/(kg $H_2O$) $RaCl_2$ and 0.25 g/(kg $H_2O$) of solid (Ba,Sr)$SO_4$ sulphate. With this total composition, the ternary solid solution becomes unstable at any composition above $x(SrSO_4) \sim 0.4$ (Fig. 8, left). At lower Sr/Ba ratios, the system behaviour is very similar to that described in the previous section, i.e. the aqueous Ra content goes through a minimum at about $x(SrSO_4) \sim 0.1$ and then steadily increases. Although the concentrations of Ra, Ba and Sr in the aqueous phase change continuously across the decomposition point, the fractions of $BaSO_4$, $RaSO_4$ and $SrSO_4$ in the solid phase experience dramatic changes at $x(SrSO_4) \sim 0.4$. The phase separation occurs through a nucleation of a minor Ba-rich phase. In the range of $0.4 < x(SrSO_4) < 0.75$ the Ba content in this phase increases despite the total content of Ba in the system decreases. At higher Sr/Ba ratios, the content of Ba in this phase decreases due to the increase of the content of $RaSO_4$, however, it remains much higher than this in the Sr-rich phase. $RaSO_4$ shows a clear preference for the Ba-rich phase. As the phase separation occurs, the content of Ra in the Sr-rich phase decreases to a very low level. An important observation is that at a certain high Sr/Ba ratio $RaSO_4$ becomes the dominant component of the Ba-rich phase.

## 3.3. Experimental equilibration of celestite with a Ra-bearing aqueous phase

### 3.3.1. Evolution of the Ra and Ba concentrations in the aqueous phase

Results of the Ra-uptake experiment show a significant decrease of the initial $^{226}Ra$ concentration in the presence of celestite (Fig. 9) - by

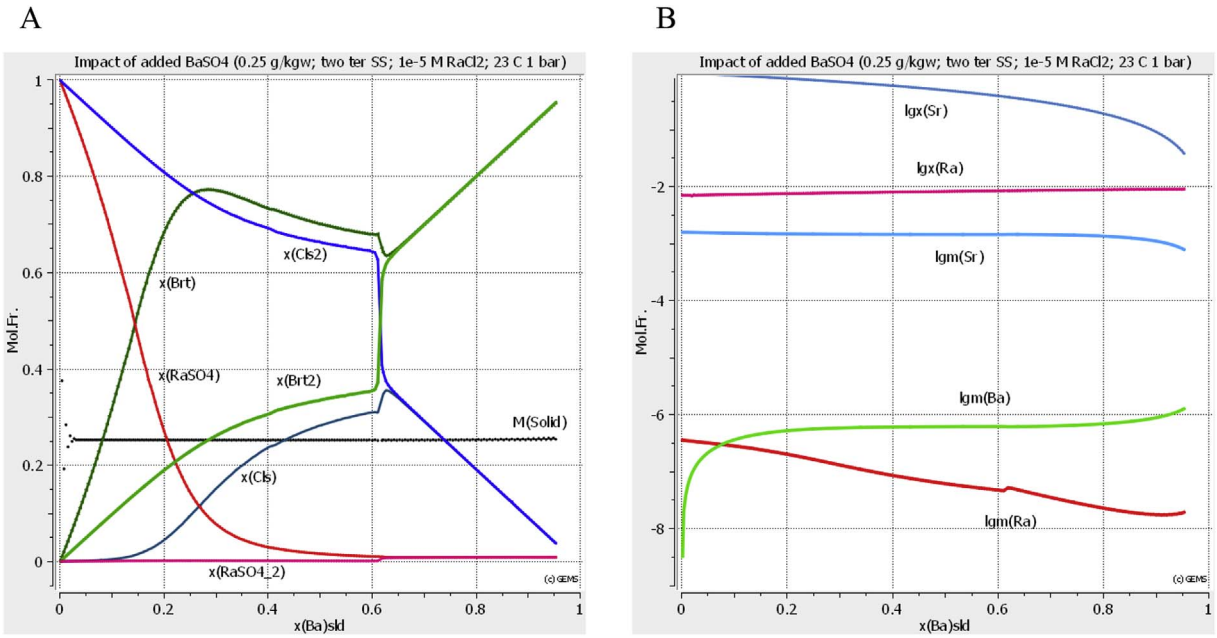


**Fig. 8.** Evolution of the composition of two ternary solid solutions Sulphate and Sulphate2 (A) and aqueous (B) phases as functions of the increase in the fraction of Ba in the system ar 23 °C, 1 bar. End members: Sulphate: Cls (celestite), Brt (barite), $RaSO_4$ (radium sulphate); Sulphate2: Cls2 (celestite), Brt2 (barite), $RaSO_4$_2 (radium sulphate). The system composition is defined by 1 kg of $H_2O$ with $1{\cdot}10^{-5}$ mol/(kg $H_2O$) $RaCl_2$ and 0.25 g/(kg $H_2O$) of solid (Ba,Sr)$SO_4$ sulphate. The figure is generated with GEM-Selektor.

more than 90%. The radium uptake appears to be connected to the release of Ba from the solid phase, where it is present in minor/trace amounts. In the presence of radium, elevated concentrations of Ba in the aqueous solution are observed, especially at the beginning of the experiment. At day 1, the aqueous Ba concentration in the Ra-containing celestite recrystallization experiment is almost one order of magnitude higher than in the Ra-free reference experiment. During the experiment, in the presence of Ra, the Ba-concentration decreases, but stays higher by a factor of ~4 compared to the Ra-free experiment, even after 828 days. Between day 226 and day 828, the concentrations of Ra, Ba and Sr in solution practically stop changing, indicating an approach to a steady state or to the equilibrium.

### 3.3.2. *Scanning electron microscopy of the equilibrated celestite*

Already at day 1, tiny idiomorphic crystals on the surface of celestite were seen, which appeared brighter in the back-scattered electron (BSE) image. If it were not for the difference in the brightness, these crystals could be easily missed in the BSE investigation. EDS analyses carried out on these crystals have shown clear peaks of Ra and Ba peaks (Fig. 10). A Ra:Ba ratio of 1:2 was typical for all analyses taken after 226 and 828 days (Table 5). These Ra-rich crystals remained present for more than 800 days (Fig. 10). On the contrary, no Ba-rich crystals were detected in the reference experiments without Ra with the same celestite sample.

## 4. Discussion

Our study provides a detailed description of the mixing properties of the ternary solid solution, which includes effects of short-range ordering. This description is based on an extensive set of ab initio calculations on supercells with single and paired substitution defects. A question is, whether this effort provided a model, which can ultimately be trusted. We argue here that our results for the sulphate solid solutions appear to be very reasonable. The set of binary *W* parameters is consistent with the observation that the main effect of non-ideality in the studied systems is determined by the size mismatch between the exchangeable cations, which is proportional to the squared volume mismatch between the end-members (Vinograd et al., 2013; Kowalski and Li, 2016). The magnitudes of pairwise ordering interactions follow the same proportionality. The strongest pairwise interactions are those

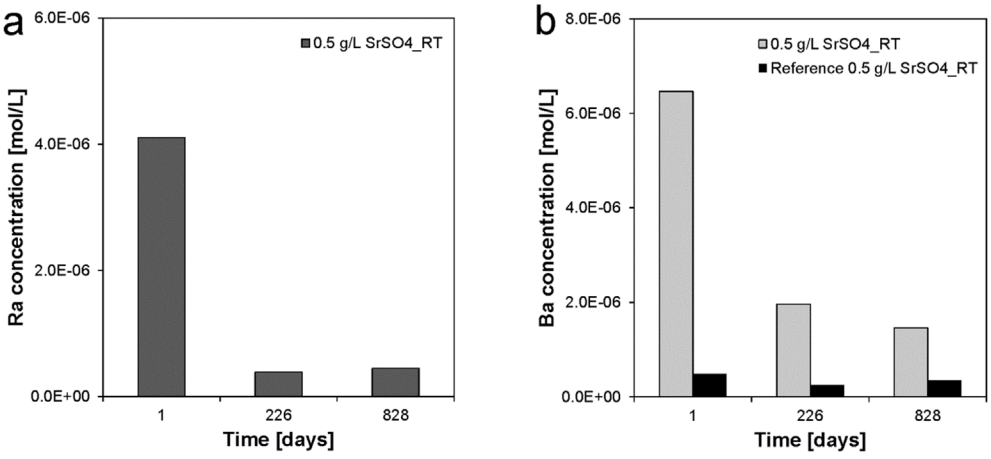


**Fig. 9.** Temporal evolution of aqueous Ra (a) and Ba (b) concentrations of 0.5 g/L experiments at room temperature.

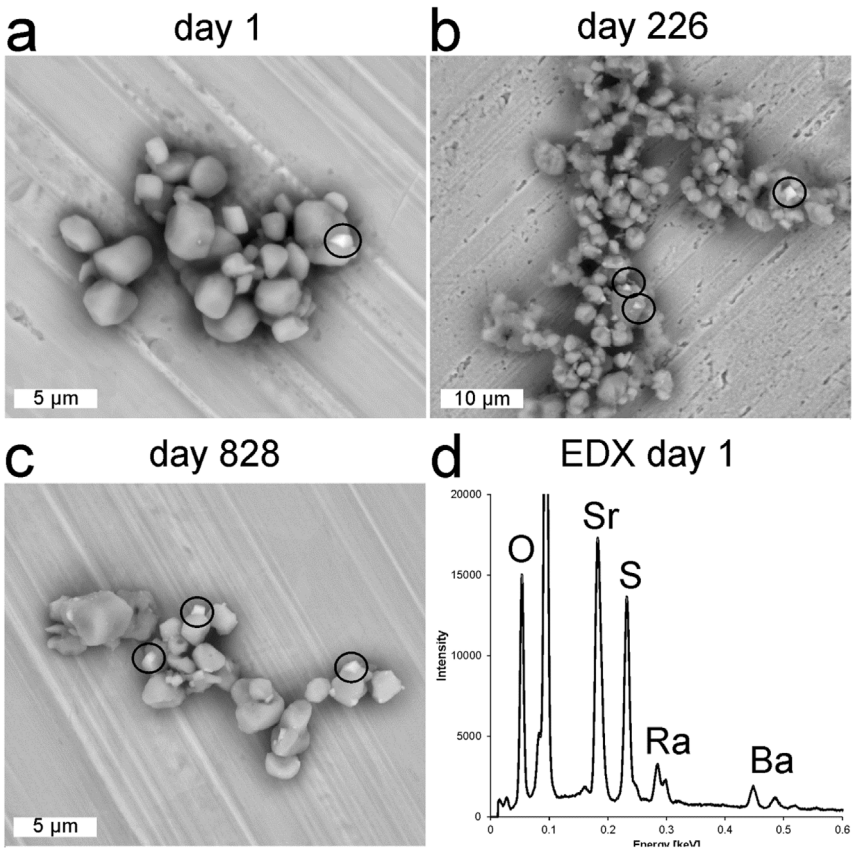


**Fig. 10.** a,b,c) SEM images of the samples of 0.5 g/L $SrSO_4$_RT put into a contact with the Ra containing solution taken after 1, 226 and 828 days, respectively. d) EDX spot measurement of a bright crystal from the sample 0.5 g/L $SrSO_4$_RT (828 days). The high Sr content is interpreted to arise from the substrate of Sr-rich crystals.

**Table 5**
Results of EDX determination of the Ra/Ba ratios of the tiny Ra-rich crystals.

| Day | Ra | Ba | Ra/Ba | Ra/Ba |
|---|---|---|---|---|
| | [at%] | [at%] | | mean value |
| 1 | 1.01 | 1.22 | 0.83 | |
| 226 | 1.28 | 2.26 | 0.57 | |
| | 0.48 | 0.97 | 0.49 | |
| | 0.78 | 2.01 | 0.39 | |
| | 0.74 | 2.00 | 0.37 | 0.45 |
| 828 | 1.01 | 1.95 | 0.52 | |
| | 2.38 | 5.47 | 0.44 | |
| | 1.38 | 2.64 | 0.52 | |
| | 0.97 | 1.76 | 0.55 | |
| | 1.54 | 3.34 | 0.46 | 0.50 |

between Ra and Sr, while the weakest are those between Ba and Ra. Although the ordering interactions are very strong in $(Ra,Sr)SO_4$, we claim that both $(Ra,Sr)SO_4$ and $(Ba,Ra)SO_4$ systems at ambient temperatures can be well described via the regular mixing model, while a special treatment based on the generalized Ising model is required only for Ba-Sr interactions, which are of intermediate strength. The reason is that in the $(Ra,Sr)SO_4$ system, the overall effect of the pairwise interactions causes a wide miscibility gap, while in the dilute limits, where the miscibility still exists, the solid solution behaves as a regular mixture. In the $(Ba,Ra)SO_4$ system, the pairwise interactions are so weak that a significant SRO occurs only at temperatures below 150 K. At higher temperatures, the solid solution is well described with the regular model. On the contrary, the pairwise interactions in the $(Ba,Sr)SO_4$ system are strong enough to cause a substantial ordering exactly in the most relevant temperature interval of 500-300 K. Therefore, their effect plays an important role in determining the miscibility ranges in the binary and in the ternary system. Our results suggest that the critical miscibility is the $(Ba,Sr)SO_4$ solid solution occurs at about 280 K. Thus, at repository conditions, we expect this solution to be fully miscible. This model is fully consistent with the wide range of barite and celestite compositions observed in Opalinus Clay formation, which experienced diagenetic conditions with temperatures about 350 K (Lerouge et al., 2014).

This model, together with the standard thermodynamic data of Ba, Sr- and Ra-sulphates and relevant aqueous species available in the PSI-Nagra database (Thoenen et al., 2014), allows an investigation of the effect of Sr in barite on Ra-uptake. Our GEM-Selektor simulations at ambient temperatures predict that Ba-Sr sulfates with intermediate Sr/(Ba + Sr) ratios are more efficient (by a factor of 7-8) for Ra-uptake compared to the case of Sr-free $BaSO_4$ barite. Our simulations, done under the assumption of reasonably large S/W ratios, show that the rocks containing celestites with less than 90% of $SrSO_4$ would still serve as very efficient Ra absorbers. Equilibrium dissolved Ra contents in pore water would be quite low due to the effect of elevated $SO_4^{2-}$ activity in the aqueous phase caused by the presence of celestite-rich sulfates.

An interesting observation can be made from the analysis of the shape of the predicted ternary miscibility gap (Fig. 6). Although the Ba-Sr binary is predicted to be fully miscible at 298 K, a small addition of $RaSO_4$ destabilizes this miscibility, such that within the ternary composition space, a phase simultaneously rich in Ba and Ra coexists with a very Sr-rich phase, which contains almost no Ra.

Our thermodynamic modelling results (Fig. 8) show that the ternary miscibility must occur in barite recrystallization experiments employing aqueous solutions containing rather low Ra activities ($10^{-6}$ m or less). The ternary phase separation is characterized by a very strong fractionation of the $RaSO_4$ component, which concentrates within a phase enriched in Ba. This effect is more pronounced at high Sr/Ba ratios, implying that an addition of Ra to the system containing a

(Ba,Sr)$SO_4$ solid solution has an effect of extracting a certain amount of $BaSO_4$ from the solid into a minor phase that tends to be rich in both Ba and Ra. At the same time, the composition of the major phase is enriched in Sr.

Our experimental results on celestite re-crystallization in the presence of a Ra-bearing aqueous solution confirm the theoretically predicted phase separation in the ternary solid solution. The observed nucleation of Ba- and Ra-rich crystals on the celestite matrix in the case of the Ra addition to the system, and the absence of such a nucleation in Ra-free experiments, corroborates the concept of phase separation, which, at high Sr/Ba ratios, requires a coexistence of Ba-Ra-rich solid solution with an almost pure celestite. Particularly interesting is the experimental observation of an increase in the Ba content of the aqueous phase upon the addition of $RaBr_2$. When no $RaBr_2$ is added, Ba happily resides within the $SrSO_4$ phase in a form of a dilute solid solution. Due to the dilution, the activity of Ba in the aqueous phase is kept very low. However, as soon as a new Ba- and Ra-rich phase is formed, the dilution effect is greatly diminished, and the aqueous content of Ba elevates significantly. This effect is observed both in our experiments and in thermodynamic simulations (Fig. 8).

On the other hand, we note that only a partial equilibrium has been achieved in our experiments. Our simulations show that the measured Ra/Ba ratio of 0.5 would require a much higher Ba/Sr ratio in the system, if the complete equilibration were assumed. Indeed, the mole fraction of $RaSO_4$ of ~1/3 in the minor phase would require $x$(Ba) ~0.2 in the newly-formed solid shown on Fig. 8. Apparently, a large fraction of celestite remained "dormant" during the equilibration. We assume that soon after the Ra–containing aqueous solution was brought into a contact with 0.5 g/L celestite, about of 60% of the solid was dissolved. This initial dissolution provided the aqueous solution with a sufficient amount of Ba,aq and $SO_4$,aq to cause the precipitation of a (Ba,Ra)$SO_4$ phase and of a certain amount of Sr-rich (Sr,Ba)$SO_4$ phase. The latter phase presumably remained undetected due to its similar SEM contrast with the bulk (unreacted) celestite. Further evolution of the system involved a gradual re-equilibration of the (Ba,Ra)$SO_4$ and (Sr,Ba)$SO_4$ phases with the initial mass of the celestite. This evolution led to an increase in the Sr-content of (Sr,Ba)$SO_4$ phase and, consequently, to a decrease in the Ra content of the (Ba,Ra)$SO_4$ phase. Indeed, the Ra/Ba ratio appears to be slightly smaller in Ra-rich crystals equilibrated for longer time intervals (Table 5). An important observation is that the tiny Ba- and Ra-rich crystals remained stable within the whole experimental time interval of 828 days. This is an indication that the phase relations in the system are governed by the ternary miscibility gap.

The observed nucleation of a Ra- and Ba-rich phase upon the interaction of a Ra-bearing solid solution with celestite has two important implications. First, our simulations and experimental results suggest a synthesis route with which very Ra-rich crystals can be crystallized from aqueous solution at a reasonably low total Ra activity. Thus, there could appear a possibility to measure certain physical properties of these crystals. Second, the predicted formation of Ra-rich crystals at high Sr/Ba ratios implies that in such systems, the dilution effect loses its important role as a factor of Ra-retention.

## 5. Conclusions

Our study provides a set of interaction parameters to describe the thermodynamics of mixing in the ternary solid solution with the barite structure. Ra mixes favourably with Ba and very unfavourably with Sr. Based on the predicted values of the Margules parameters, ($W_{BaRa}$ = 2.47 ± 0.22, $W_{BaSr}$ = 4.95 ± 0.75 and $W_{SrRa}$ = 17.50 ± 1.40 kJ/mol), an addition of $RaSO_4$ to the (Ba,Sr)$SO_4$ binary solid solution would stabilize a Ba-rich phase and destabilize a Sr-rich phase. The effects of short-range order appear to be especially important in the (Ba,Sr)$SO_4$ binary system. The model predicts complete mixing in the Ba-Ra and Ba-Sr binaries at and above 25 °C and a large miscibility gap in the Ra-Sr binary. This gap significantly expands into the ternary composition space.

GEM-Selektor calculations of equilibria in the (Ba,Sr,Ra)$SO_4$ SS-AS systems show that, in agreement with previous experimental and theoretical studies, an increase in the host solid-water mass ratio is always a positive factor for Ra uptake. An important prediction made in the present study is that a moderate increase in the Sr/Ba ratio leads to an even stronger Ra retention: the presence of $SrSO_4$ in the solid solution up to 5–10 mol % reduces the dissolved Ra,aq concentration by factor of 7–8 compared to the previously studied SS-AS systems containing no $SrSO_4$ (e. g. Bosbach et al., 2010; Curti et al., 2010; Klinkenberg et al., 2014; Brandt et al., 2015). However, a further increase in the Sr/Ba ratio makes Ra retention less effective. The latter effect has been modelled in SS-AS systems both with and without phase separation. In systems with low Ra loading, there is a complete mixing within the ternary solid phase, (Ba,Sr,Ra)$SO_4$, containing a trace amount or $RaSO_4$. In this case, the uptake of Ra into the solid decreases due to the dependence of $\gamma(RaSO_4)$ on $W_{SrRa}$. On the other hand, in systems, in which the fraction of $SrSO_4$ is close to one, a minor amount of $RaSO_4$ causes a phase separation. A phase, which is simultaneously rich in Ba and Ra then coexists with a nearly pure celestite. The Ra/Ba ratio in the barium-rich phase increases with the increase of the Sr/Ba ratio in the system. In such a system, a reduction in Ra-retention is primarily caused by an increase in the mole fraction of $RaSO_4$ $x(RaSO_4)$, which makes the dilution effect less effective.

The results of the present study significantly improve our understanding of efficiencies of natural types of barite in Ra retention. These results benefited from new atomistic approaches to study the thermodynamics of mixing in solid solutions, which are, in turn, based on the recent progress in first-principles calculations, and from the use of advanced Gibbs energy minimization algorithms, adapted to ternary mixtures, as implemented within the GEM-Selektor package (http://gems.web.psi.ch). The ultimate validation of our results has been provided by a direct experimental study of Ra-uptake, which required precise measurements on samples with rather high radioactivity.

## Acknowledgements

The research leading to these results has received partial funding from the German Federal Ministry of Education and Research (BMBF) (joint projects ImmoRad (grant 02NUK019) and ThermAc3 (grants 02NUK039)) and from Deutsche Forschungsgemeinschaft (DFG) (grant VI-196/2-1 and Wi 1232/44-1). DK is grateful to Nagra, Wettingen, for partial financial support. The atomistic computations were performed at the Jülich Supercomputing Centre.

## Appendix

### *A1. Consequences of instability of Pnma $SrSO_4$ in DFT calculations*

Visual analysis of the converged structures with the composition of $Ba_2Sr_{30}(SO_4)_{32}$, whose Ba-Ba distances correspond to $n$ = 3, 5 and 6, revealed that they adopted a relaxation mechanism, in which each $SO_4$ tetrahedron is rotated by about 7° relative to its ideal position in the orthorhombic structure. The regular alternating pattern of rotations is best observed in the projection onto the *a-b* plane (Fig. A1). The supercell structures with the composition of $Sr_{32}(SO_4)_{32}$ obtained from the supercells with $n$ = 3, 5 and 6 by a reverse substitution of two Ba atoms by Sr atoms upon geometric

relaxation converged into a monoclinic, $P2_1/n$, structure, in which the regular rotation of the tetrahedra remained as the stable feature. The $P2_1/n$ structure appeared to be more stable than the orthorhombic one by about 0.072 eV per formula unit. This observation suggests that the very different excess energies of the structures with double defects at the 3, 5 and 6 defect-defect distances (Fig. 4, right) are caused by an instability of the orthorhombic $SrSO_4$ in the athermal limit relative to the monoclinic form. Apparently, the transition to the monoclinic structure is triggered by double BaBa defects placed along certain directions. The other double defect structures, which didn't reveal the peculiar relaxation mechanism, apparently remained metastable relative to the orthorhombic/monoclinic transition. Interestingly, the single-defect structure of $BaSr_{31}(SO_4)_{32}$ also did not show any sign of the monoclinic distortion on relaxation. This metastability, in fact, allowed us to compute the $W_{BaSr/Sr}$ and $W_{SrRa/Sr}$ parameters, which are consistent with the orthorhombic symmetry.

The relative stabilities of the $P2_1/n$ and Pnma forms of $SrSO_4$ were also investigated with the modified force-field model of Allan et al. (1993). Contrary to the DFT calculations, the force-field calculations predicted the $P2_1/n$ form to be less stable than the orthorhombic one. Even when the force-field geometry optimization starts from the $P2_1/n$ structure, the final result is the Pnma barite. The predicted metastability of the Pnma $SrSO_4$ requires a further investigation. Possibly, it occurs just within the adopted DFT computational scheme. Since we were interested in the mixing properties of the solid solution relative to barite-type endmembers, the supercell structures that reflected the stability of the $P2_1/n$ structure were excluded from any further analysis. Consequently, the present analysis of mixing effects in the $(Ba,Sr)SO_4$ binary is based only on the supercell structures with SrSr defects in $BaSO_4$. The same problem prevented the computation of the barite-type pairwise interactions from the structures with RaRa defects in $SrSO_4$.

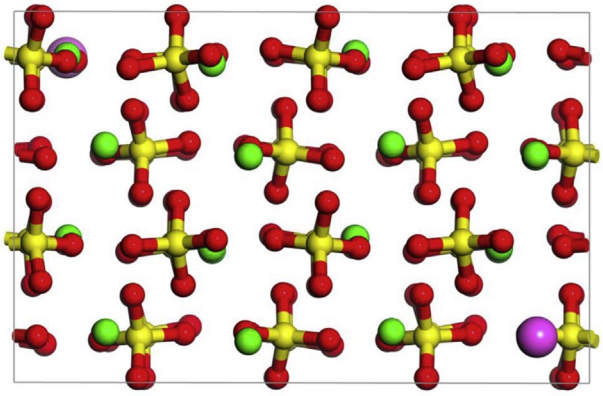

**Fig. A1.** Converged geometry of a 2 × 2 × 2 supercell of celestite with a pair of Ba defects (pink spheres) at the third distance ($n$ = 3) in the projection onto the $a$-$b$ plane. Note the regular pattern of rotations of the $SO_4$ tetrahedra. This pattern is consistent with a monoclinic structure of $SrSO_4$.

### *A2. The ternary interaction parameter*

In this study, a special care was taken to estimate the value of the ternary interaction parameter in Eqn. (13). Based on the cation size argument, one could assume that an admixture of $Ba^{2+}$ to the equal mixture of $Sr^{2+}$ and $Ra^{2+}$ would cost less energy than it is predicted with the ternary regular model, because the size of $Ba^{2+}$ is almost equal to the average of the sizes of $Sr^{2+}$ and $Ra^{2+}$. This argument would suggest that $W_{BaSrRa}$ could be negative. To test this hypothesis, a set of 21 ternary quasi-random structures was simulated, and their excess enthalpies were computed with the force-field method. Fig. A2 shows the correlation between the enthalpy of mixing computed directly via the static energy minimization with GULP and the enthalpy predicted with Eqn. (13) with $W_{IJK} = 0$. Two models were tested. In the first case, the average $W_{IJ}$ parameters were used as required by the regular mixing, while in the second case, the subregular behaviour was assumed in the binaries. Each ternary composition was represented either by 3 or 6 different QRS, and their average enthalpies were plotted. The observed linear correlations imply that the enthalpy of ternary mixing is accurately predicted via Eqn. (13) under the assumption that the interaction parameter is zero. If the ternary interactions were present, it would be impossible to match the enthalpies of ternary quasi-random structures via Eqn. (13) and $W_{BaSrRa} = 0$.

Rigorously, these results only show that no ternary interaction parameter is required in the force-field model of the ternary mixture. However, the good match between the binary $W$ parameters computed from DFT and the force-field model together with the apparent linear correlation between the both sets of these parameters and the relative squared volume difference of the endmembers (Vinograd et al., 2013), suggests that the excess energies are primarily of elastic origin and the force-field model should be sufficiently robust in the description of energy vs, size relationship. Thus, we could be reasonably confident that a specific ternary interaction parameter is not needed. Fig. A2 shows also that the subregular model gives almost no advantage relative to the regular one. This is the consequence of the similarity between $W_{IJ/I}$ and $W_{IJ/J}$ parameters in all binary systems studied here. Practically, this means that the subregular ternary model for $(Ba,Sr,Ra)SO_4$ would give almost no increase in the accuracy over the regular one.

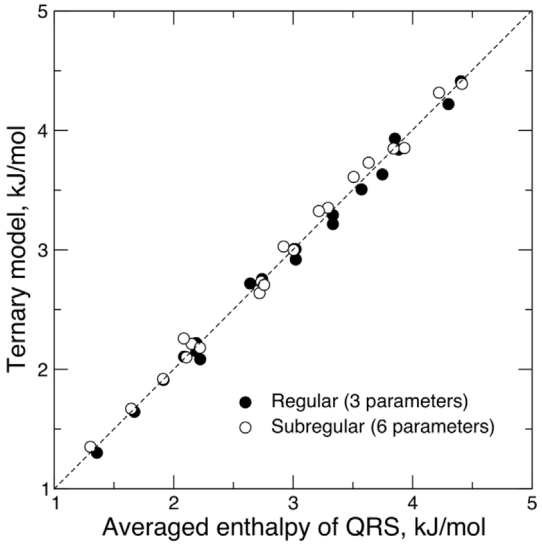


**Fig. A2.** The enthalpy of mixing in the ternary regular (subregular) solid solution parameterized via the Margules parameters of the binary systems vs. the excess enthalpy of a quasi-random structure.

*A3 Parameters of the generalized Ising model for ternary sulphates*

Table A1
Degeneracy numbers and coordination numbers in a $2 \times 2 \times 2$ supercell as a function of the order of neighbors.

| $n$ | $D_n$ | $Z_n$ |
|---|---|---|
| 1 | 1 | 2 |
| 2 | 1 | 4 |
| 3 | 1 | 2 |
| 4 | 2 | 2 |
| 5 | 1 | 2 |
| 6 | 1 | 2 |
| 7 | 2 | 4 |
| 8 | 2 | 2 |
| 9 | 1 | 2 |
| 10 | 1 | 2 |
| 11 | 2 | 2 |
| 12 | 1 | 4 |
| 13 | 4 | 4 |
| 14 | 2 | 4 |
| 15 | 4 | 4 |
| 16 | 4 | 4 |
| 17 | 8 | 8 |

Table A2
The pairwise interactions derived from DFT calculations and used in Monte Carlo simulations of the ternary mixing

| BaBa + SrSr = 2BaSr: | | | | |
|---|---|---|---|---|
| $n$ | $d$(Å) | $J_{BaSr/Ba}$ | $J_{BaSr/Sr}$ | $J_{BaSr/Ra}$ |
| 1 | 4.624 | −3.27172 | −2.8704 | −3.07106 |
| 2 | 4.643 | 5.3241 | 4.6710 | 4.9975 |
| 3 | 4.824 | 2.09079 | 1.83433 | 1.9626 |
| 4 | 5.450 | −2.54768 | −2.23518 | −2.39143 |
| 5 | 6.479 | −0.05816 | −0.05103 | −0.05459 |
| 6 | 6.626 | −0.25531 | −0.22399 | −0.23965 |
| 7 | 7.147 | 0.08428 | 0.07394 | 0.07910 |
| 8 | 7.150 | −0.70432 | −0.61793 | −0.66113 |

| | | | | |
|---|---|---|---|---|
| 9 | 7.335 | −0.05816 | −0.05103 | −0.05459 |
| 10 | 7.912 | 1.47962 | 1.2981 | 1.38887 |
| 11 | 8.870 | 0.32086 | 0.2815 | 0.30118 |
| 12 | 8.922 | 0.27610 | 0.24302 | 0.26001 |
| 13 | 8.990 | 0.37730 | 0.33102 | 0.35416 |
| 14 | 9.138 | 0.10893 | 0.09556 | 0.10225 |
| 15 | 10.410 | −0.19937 | −0.17492 | −0.18714 |
| 16 | 11.393 | −0.19198 | −0.16843 | −0.18020 |
| 17 | 12.629 | 0.07775 | 0.06821 | 0.07299 |

BaBa + RaRa = 2BaRa:

| *n* | *d*(Å) | $J_{BaRa/Ba}$ | $J_{BaRa/Ra}$ | $J_{BaRa/Sr}$ |
|---|---|---|---|---|
| 1 | 4.624 | −0.32100 | −0.38114 | −0.35550 |
| 2 | 4.643 | 0.40871 | 0.89917 | 0.65394 |
| 3 | 4.824 | 0.27083 | 0.01280 | 0.14182 |
| 4 | 5.450 | −0.29792 | −0.33830 | −0.31811 |
| 5 | 6.479 | −0.02462 | 0.01280 | −0.00591 |
| 6 | 6.626 | 0.17235 | 0.11129 | 0.14182 |
| 7 | 7.147 | 0.11572 | 0.05564 | 0.08568 |
| 8 | 7.150 | −0.03201 | −0.14133 | −0.08667 |
| 9 | 7.335 | 0.21174 | 0.20978 | 0.21076 |
| 10 | 7.912 | 0.32008 | 0.30826 | 0.31417 |
| 11 | 8.870 | 0.31116 | 0.05564 | 0.18340 |
| 12 | 8.922 | 0.16250 | 0.11129 | 0.13689 |
| 13 | 8.990 | 0.12926 | 0.10169 | 0.11547 |
| 14 | 9.138 | 0.11572 | 0.05564 | 0.08568 |
| 15 | 10.410 | −0.04063 | −0.04604 | −0.04333 |
| 16 | 11.393 | 0.04309 | 0.00320 | 0.02314 |
| 17 | 12.629 | 0.02154 | 0.02622 | 0.02388 |

SrSr + RaRa = 2SrRa:

| *n* | *d*(Å) | $J_{SrRa/Sr}$ | $J_{SrRa/Ra}$ | $J_{SrRa/Ba}$ |
|---|---|---|---|---|
| 1 | 4.624 | −5.15053 | −5.25729 | −5.20391 |
| 2 | 4.643 | 9.56539 | 9.76367 | 9.66453 |
| 3 | 4.824 | 3.94147 | 4.02317 | 3.98232 |
| 4 | 5.450 | −3.74691 | −3.82458 | −3.78575 |
| 5 | 6.479 | 0.09846 | 0.10050 | 0.09948 |
| 6 | 6.626 | 0.28593 | 0.29185 | 0.28889 |
| 7 | 7.147 | −0.32570 | −0.33245 | −0.32907 |
| 8 | 7.150 | −0.98182 | −1.00217 | −0.99200 |
| 9 | 7.335 | −0.27646 | −0.28220 | −0.27933 |
| 10 | 7.912 | 3.00415 | 3.06642 | 3.03529 |
| 11 | 8.870 | 0.14296 | 0.14593 | 0.14445 |
| 12 | 8.922 | 0.37966 | 0.38753 | 0.38359 |
| 13 | 8.990 | 0.84477 | 0.86228 | 0.85353 |
| 14 | 9.138 | 0.93969 | 0.95916 | 0.94942 |
| 15 | 10.410 | −0.42061 | −0.42933 | −0.42497 |
| 16 | 11.393 | 0.04805 | 0.04904 | 0.04855 |
| 17 | 12.629 | 0.12947 | 0.13217 | 0.13081 |

## References


Allan, N.L., Rohl, A.L., Gay, D.H., Catlow, R.A., Davey, R.J., Mackrodt, W.C., 1993. Calculated bulk and surface properties of sulfates. Faraday Discuss. 95, 1–7.

Becker, U., Fernández-González, A., Prieto, M., Harrison, R., Putnis, A., 2000. Direct calculations of thermodynamic properties of the barite-celestite solid solution from molecular principles. Phys. Chem. Miner. 27, 291–300.

Bosbach, D., Boettle, M., Metz, V., 2010. Experimental Study on $Ra^{2+}$ Uptake by Barite BaSO4 Kinetics of Solid Solution Formation via $BaSO_4$ Dissolution and $Ra_xBa_{1-x}SO_4$ Reprecipitation. Technical Report TR-10–14. Svensk Kärnbränslehantering AB Swedish Nuclear Fuel and Waste Management Company.

Brandt, F., Curti, E., Klinkenberg, M., Rozov, K., Bosbach, D., 2015. Replacement of barite by a $(Ba,Ra)SO_4$ solid solution at close-to-equilibrium conditions: a combined experimental and theoretical study. Geochimica et Cosmochimica Acta 155, 1-15.

Ceccarello S., Black S., Read D., Hodson M. E. (2004) Industrial radioactive barite scale: suppression of radium uptake by introduction of competing ions. Miner. Eng. 17 (2), 323–330.

Brower, E., Renault, J., 1971. Solubility and enthalpy of the barium-strontium sulfate solid solution series. N. M. State Bur. Mines Miner. Resour. Circular 116, 1–21.

Bruno, J., Ewing, R.C., 2006. Spent nuclear fuel. ELEMENTS 2, 343–349.

Bruno, J., Bosbach, D., Kulik, D., Navrotsky, A., 2007. Chemical thermodynamics of solid solutions of interest in radioactive waste management: a state-of-the art report. In: Mompean, F.J., Illemassene, M., Perrone, J. (Eds.), Chemical Thermodynamics Series, V. 10. OECD, Paris, pp. 6–100.

Clark, S.J., Segall, M.D., Pickard, C.J., Hasnip, P.J., Probert, M.J., Refson, K., Payne, M.C., 2005. First principles methods using CASTEP. Z. für Kristallogr. 220, 567–570.

Curti, E., Fujiwara, K., Iijima, K., Tits, J., Cuesta, C., Kitamura, A., Glaus, M., Müller, W.,

2010. Radium uptake during barite recrystallization at 23 ± 2°C as a function of solution composition: an experimental $^{133}$Ba and $^{226}$Ra tracer study. Geochim. Cosmochim. Acta 74, 3553–3570.
Dove, M.T., 1993. Introduction to Lattice Dynamics. CUP. ISBN-13: 978–0521392938.
Gale, J.D., Rohl, A.L., 2003. The general utility lattice program (GULP). Mol. Simul. 29, 291–341.
Galinier, C., Dandurand, F., Souissi, J., Schott, J., 1989. Non-ideal behavior of (Ba,Sr)$SO_4$ crystalline solutions-Determination of the mixing properties by dissolution runs at 25 °C. C.R. Acad. Sci. Ser. II 308, 1363–1368.
Ganguly, J., 2001. Thermodynamic modeling of solid solutions. In: In: Geiger, ChA. (Ed.), Solid Solutions in Silicate and Oxide Systems. EMU Notes in Mineralogy, vol. 3. EÖTVÖS University Press, Budapest, pp. 37–69 (Chapter 3).
Grandia, F., Merino, J., Bruno, J., 2008. Technical Report TR- 08–07: Assessment of the Radium–barium Co-precipitation and its Potential Influence on the Solubility of Ra in the Near-field. Svensk Kärnbränsle-hantering AB. Swedish Nuclear Fuel and Waste Management Company, Sweden.
Hanor, J.S., 2000. Barite-celestine geochemistry and environments of formation. In: Alpers, C.N., Jambor, J.L., Nordstrom, D.K. (Eds.), Reviews in Mineralogy. Sulfate Minerals, vol 40. Mineralogical Society of America, pp. 193–276.
Helgeson, H.C., Kirkham, D.H., Flowers, G.C., 1981. Theoretical prediction of the thermodynamic behavior of aqueous electrolytes at high pressures and temperatures: IV. Calculation of activity coefficients, osmotic coefficients and apparent and standard and relative partial molal properties to 600 _C and 5 kb. Am. J. Sci. 281, 1249–1516.
Heberling, F., Schild, D., Degering, D., Schäfer, T., 2017. How well suited are current thermodynamic models to predict or interpret the composition of (Ba,Sr)$SO_4$ solid-solutions in geothermal scalings? Geotherm. Energy 5, 9. http://dx.doi.org/10.1186/s40517-017-0068-x.
Hildebrand, J.H., 1929. Solubility, XII. Regular solutions. J. Am. Chem. Soc. 51, 66–80.
Hoshino, T., Schweika, W., Zeller, R., Dederichs, P.H., 1993. Impurity–impurity interactions in Cu, Ni, Ag, and Pd. Phys. Rev. B 47, 5106–5117.
Hummel, W., Berner, U., Curti, E., Pearson, F.J., Thoenen, T., 2002. Nagra/PSI Chemical Thermodynamic Data Base 01/01. Nagra technical report 02–16. .
Jacobsen, S.D., Smyth, J.R., Swope, R.J., Downs, R.T., 1998. Rigid-body character of the $SO_4$ groups in celestine, anglesite and barite. Can. Mineral. 36, 1053–1060.
Johnson, J.W., Oelkers, E.H., Helgeson, H.C., 1992. SUPCRT92: a software package for calculating the standard molal thermodynamic properties of minerals, gases, aqueous species, and reactions from 1 to 5000 bar and 0 to 1000°C. Comp. Geosci. 18, 899–947.
Klinkenberg, M., Brandt, F., Breuer, U., Bosbach, D., 2014. Uptake of Ra during the recrystallization of barite: a microscopic and time of flight-secondary ion mass spectrometry study. Environ. Sci. Technol. 48, 6620–6627.
Kowalski, P.M., Li, Y., 2016. Relationship between the thermodynamic excess properties of mixing and the elastic moduli in the monazite-type ceramics. J. Eur. Ceram. Soc. 36, 2093–2096.
Kulik, D.A., Berner, U., Curti, E., March 2004. Modelling chemical equilibrium partitioning with the GEMS-PSI code. In: Smith, B., Gschwend, B. (Eds.), PSI Scientific Report 2003/Volume IV, Nuclear Energy and Safety. Paul Scherrer Institute, Villigen, Switzerland, pp. 109–122 (ISSN 1423-7334).
Kulik, D.A., Wagner, T., Dmytrieva, S.V., Kosakowski, G., Hingerl, F.F., Chudnenko, K.V., Berner, U., 2013. GEMSelektor geochemical modeling package: revised algorithm and GEMS3K numerical kernel for coupled simulation codes. Comput. Geosci. 17, 1–24.
Lerouge, C., Grangeon, S., Gaucher, E.C., Tournassat, C., Agrinier, P., Guerrot, C., Widory, D., Flehoc, C., Wille, G., Ramboz, C., Vinsot, A., Buschaert, S., 2011. Mineralogical and isotopic record of biotic and abiotic diagenesis of the Callovian-Oxfordial clayey formation of Bure (France). Geochem. Cosmochem. Acta 75, 2633–2663.
Lerouge, C., Grangeon, S., Claret, F., Gaucher, E.C., Blanc, Ph, Guerrot, C., Flehoc, Chr, Wille, G., Mazurek, M., 2014. Mineralogical and isotopic record of diagenesis from the Opalinus Clay formation at Benken, Switzerland: implications for the modeling of pore-water chemistry in a clay formation. Clays clay Miner. 62 (4), 286–312.
Liu, X., Vinograd, V.L., Lu, X., Leonenko, E.V., Eremin, N.N., Wang, R., Winkler, B., 2016. Thermodynamics of mixing in an isostructural solid solution: simulation methodologies and application to the rutile-cassiterite system. Am. Mineral. 101, 1197–1206.
Malinin, S.D., Urusov, V.S., 1983. The experimental and theoretical data on isomorphism in the (Ba, Sr)$SO_4$ system in relation to barite formation. Geokhimiya 9, 1324–1334.
Metropolis, N., Rosenbluth, A.W., Rosenbluth, M.N., Teller, A.H., Teller, E., 1953. Equation of state calculations by fast computing machines. J. Chem. Phys. 21, 1087–1092.
NAGRA, December 1984. Technical Report 84–32. An Assessment of the Corrosion Resistance of the High-level Waste Containers Proposed by NAGRA. The Nagra Working Group on Container Technology.
NAGRA, 2014. Technischer bericht NTW 14-03. Charakt. Dosisintervalle Unterlagen zur Bewert. Barrierensysteme 1–61 ISSN 1015–2636.
Prieto, M., Heberling, F., Rodríguez-Galán, R.M., Brandt, F., 2016. Crystallization behavior of solid solutions from aqueous solutions: an environmental perspective. Prog. Cryst. Growth Charact. Mater. 62, 29–68.
SKB, 2011. Technical Report TR-11-01. Long-term safety for the final repository for spent nuclear fuel at Forsmark. Main report of the SR-Site project Volume III. Sven. Kärnbränslehantering Ab. 563–893 March 2011. ISSN 1404–0344.
Sluiter, M.H.F., Kawazoe, Y., 2002. Prediction of mixing enthalpy of alloys. Europhys. Lett. 57, 526–532.
Thoenen, T., Hummel, W., Berner, U., Curti, E., 2014. The PSI/Nagra Chemical Thermodynamic Database 12/07. PSI Bericht Nr. 14-04. ISSN 1019–0643.
Vinograd, V.L., Sluiter, M.H.F., Winkler, B., 2009. Subsolidus phase relations in the $CaCO_3$-$MgCO_3$ system predicted from the excess enthalpies of supercell structures with single and double de-fects. Phys. Rev. B 79, 104209.
Vinograd, V.L., Paulsen, N., Winkler, B., van de Walle, A., 2010. Thermodynamics of mixing in the ternary rhombohedral carbonate solid solution ($Ca_xMg_yMn_{1-x-y}$)$CO_3$ from atomistic simulations. CALPHAD 34, 113–119.
Vinograd, V.L., Brandt, F., Rozov, K., Klinkenberg, M., Refson, K., Winkler, B., Bosbach, D., 2013. Solid–aqueous equilibrium in the $BaSO_4$–$RaSO_4$–$H_2O$ system: first-principles calculations and a thermodynamic assessment. Geochim. Cosmochim. Acta 122, 398–417.
Vinograd, V.L., Kulik, D.A., Brandt, F., Klinkenberg, M., Winkler, B., Bosbach, D., 2017. Thermodynamics of the solid solution - aqueous solution system (Ba,Sr,Ra)$SO_4$ + $H_2O$: II. Radium retention in barite-type minerals at elevated temperatures. Appl. Geochem. http://dx.doi.org/10.1016/j.apgeochem.2017.10.019. Online: 20-NOV-2017.
Wagner, T., Kulik, D.A., Hingerl, F.F., Dmytrieva, S.V., 2012. GEM-Selektor geochemical modeling package: TSolMod library and data interface for multicomponent phase models. Can. Mineral. 50, 1173–1195.
Warren, M.C., Dove, M.T., Myers, E.R., Bosenick, A., Palin, E.J., Sainz-Diaz, C.I., Guiton, B.S., Redfern, S.A.T., 2001. Monte Carlo methods for the study of cation ordering in minerals. Mineral. Mag. 65, 221–248.
Weber, J., Barthel, J., Klinkenberg, M., Bosbach, D., Kruth, M., Brandt, F., 2017. Retention of $^{226}$Ra by Barite: the Role of Internal Porosity. (accepted for publication in Chemical Geology).
Weigel, F., Trinkl, A., 1973. Crystalline chemistry of radium. 5. Diverse radium salts of inorganic anions. Radiochim. Acta 19, 199–202.
Wohl, K., 1946. Thermodynamic evaluation of binary and ternary liquid systems. Trans. Am. Inst. Chem. Eng. 42, 215–249.
Wu, Z.G., Cohen, R.E., 2006. More accurate generalized gradient approximation for solids. Phys. Rev. B 73, 235116.
Zhu, C., 2004. Coprecipitation in the Barite isostructural family: 1. Binary mixing properties. Geochim. Cosmochim. Acta 68, 3327–3337.
Zunger, A., Wei, S., Ferreira, L.G., Bernard, J.E., 1990. Special quasirandom structures. Phys. Rev. Lett. 65 (3), 353–356.